Gravitational redshift in clusters of galaxies

Master thesis by

Solveig Witting
Dark Cosmology Centre
Niels Bohr Institute
Faculty of Science
University of Copenhagen

Supervisors

Jens Hjorth
and
Jesper Sommer-Larsen

July 2006

Contents

1 Introduction **1**
- 1.1 Theory . . . 1
  - 1.1.1 Gravitational redshift . . . 1
  - 1.1.2 Gravitational redshift in clusters of galaxies . . . 3
- 1.2 Review of previous work . . . 4
- 1.3 The possible approaches . . . 6
- 1.4 Thesis outline . . . 7

2 Analytical estimates of the effect **9**
- 2.1 The Hernquist profile . . . 9
- 2.2 The NFW-profile . . . 13
- 2.3 The number of available clusters . . . 16

3 The simulations **21**
- 3.1 The simulation method . . . 21
  - 3.1.1 Group finding . . . 23
- 3.2 Results from simulations . . . 24

4 The data and the method of data selection **29**
- 4.1 The data samples . . . 29
  - 4.1.1 The RASS-SDSS . . . 29
  - 4.1.2 The Abell samples . . . 31
- 4.2 Member galaxy selection . . . 31
  - 4.2.1 Scaling of the RASS-SDSS sample . . . 37

5 Results **43**
- 5.1 The RASS-SDSS . . . 46
- 5.2 The Abell samples . . . 52

6 The Movement of the cD **59**
6.1 Formation of cD-galaxies 59
6.2 Studies of cD peculiar velocities 61
6.3 The movement of non-cD BCGs 62
6.4 Peculiar velocities of the three applied samples 65

7 Summary and discussion **69**
7.1 Summary 69
7.2 Discussion 70

8 Appendix A: The NFW-distribution **75**

Chapter 1

Introduction

Since Oort's initial discovery of the Galaxy's missing matter problem in the 1930s, the question of dark matter has been one of the major puzzles of modern cosmology.

The problem has been attacked from a number of different angles and a wide spectrum of methods has been applied in attempts to gauge the nature, the origin and the distribution of the dark matter.

Obtaining a clearer picture of the relationship between the spatial distribution of dark and luminous matter, might constitute a critical step in solving the dark matter problem and might also be of central importance for understanding the growth of structure in the universe. It therefore seems worth the effort, to develop methods that can probe the matter distribution in large-scale structures.

In this thesis I will explore the possibility of measuring the effect of gravitational redshift in clusters of galaxies as a way to determine the mass distributions of these structures.

1.1 Theory

1.1.1 Gravitational redshift

Consider a photon moving out of a gravitational field. The photon will experience a loss of energy as it makes its way out of the field and this will be visible as a redshift in its frequency. This effect is called a gravitational redshift and can be understood from the following derivations.

Looking at a gravitational field, with an arbitrary time independent metric, the square of an interval between two events has the following general expression

$$ds^2 = g_{ik}dx^i dx^k \tag{1.1}$$

where the g's are the components of the metric tensor. Since the metric is assumed to be time independent, the square of the interval between to purely timelike events is given by

$$ds^2 = c^2 d\tau^2 = g_{00}c^2(dx^0)^2 \tag{1.2}$$

where $d\tau$ is the proper time interval between the two events. Consider now the two proper time intervals between two photons leaving the locations $\mathbf{r_1}$ and $\mathbf{r_2}$ respectively. From the above it is clear that these two intervals can be expressed as

$$d\tau_1^2 = g_{00}(\mathbf{r_1})(dx^0)^2 \tag{1.3}$$
$$d\tau_2^2 = g_{00}(\mathbf{r_2})(dx^0)^2 \tag{1.4}$$

where dx^0 is the same in both expressions, because of the time independence of the metric. The proper frequency's is defined as

$$\nu_i = \frac{1}{d\tau_i} \tag{1.5}$$

and from this it follows that the ratio of the frequencies measured in $\mathbf{r_1}$ and $\mathbf{r_2}$ respectively will be given by

$$\frac{\nu_2}{\nu_1} = \sqrt{\frac{g_{00}(\mathbf{r_1})}{g_{00}(\mathbf{r_2})}} \tag{1.6}$$

The metric tensor is related to the potential through the following expression

$$g_{00}(\mathbf{r}) = 1 + \frac{2 * \Phi(\mathbf{r})}{c^2} \tag{1.7}$$

and this implies that the redshift can be expressed as

$$z = \frac{\nu_2 - \nu_1}{\nu_1} \tag{1.8}$$

$$= \sqrt{\frac{1+\frac{2*\Phi(\mathbf{r_1})}{c^2}}{1+\frac{2*\Phi(\mathbf{r_2})}{c^2}} - 1} \tag{1.9}$$

$$= \frac{\phi(\mathbf{r_1})}{c^2} - \frac{\phi(\mathbf{r_2})}{c^2} - \frac{\phi(\mathbf{r_1}) * \phi(\mathbf{r_2})}{c^4} - \frac{\phi(\mathbf{r_1})^2}{2c^4} + \frac{3 * \phi(\mathbf{r_2})^2}{2c^4} + \cdots \tag{1.10}$$

where the last equality is achieved by taking the product of Taylor expansion of denominator and the numerator in the preceding expression.

Neglecting the higher order terms, which can be done since $\frac{\Phi(\mathbf{r})}{c^2} \leq 1$, we get that

$$z \simeq \frac{\phi(\mathbf{r_1})}{c^2} - \frac{\phi(\mathbf{r_2})}{c^2} \tag{1.11}$$

If one assumes that $|\Phi(\mathbf{r_2})| \ll |\Phi(\mathbf{r_1})|$ then

$$z \simeq \frac{\phi(\mathbf{r_1})}{c^2} \tag{1.12}$$

and from this it follows that the velocity v_g associated with the gravitational redshift can be defined as

$$v_g \simeq -\frac{\phi(\mathbf{r_1})}{c} \tag{1.13}$$

1.1.2 Gravitational redshift in clusters of galaxies

From the above it becomes clear, that the effect of gravitational redshift is a measure of the depth and the steepness of the gravitational well associated with a given matter distribution. As a result the effect can be used to obtain information about the shape of the distribution. By measuring the redshift as a function of radius in a galaxy cluster, it should theoretically be possible to fit a profile to the mass distribution of the cluster. The size of the effect of gravitational redshift will depend on the total mass of the cluster and on the degree of central concentration of the matter distribution.

In reality the measurement of the effect is not easily managed. As will be shown in chapter 2 and 3, the expected size of the effect will range from about 5 to 60 km/s, which is significantly smaller than the Doppler shifts associated with the random movements of the galaxies in an average cluster. Furthermore other sources of noise for instance given by velocities caused by cluster substructure might make it even harder to measure the effect.

1.2 Review of previous work

The subject of gravitational redshift in galaxies and galaxy clusters has been the purpose of several studies in the last 30 years.

- As early as in 1976 Nottale [19] found an apparent correlation between cluster richness and redshift differences, when comparing pairs of clusters with different richness. 17 out of 22 pairs of galaxy groups and clusters showed a positive difference in redshift between the richer and the poorer members of the pair.

- In 1982 Rood and Struble [27] repeated the test with a larger sample of 84 pairs, but without being able to confirm the result. They found no correlation between redshift and richness difference within observational and statistical uncertainties at the $1-\sigma$ level.

- In 1993 Stiavelli and Setti (S&S) [32] measured the effect in a sample of elliptical galaxies by separating the radial velocity profiles in odd and even components with respect to the galaxy centre. If the even component has non-zero values, these can supply information on systematic non-equilibrium motion in the galaxy. S&S measure the non-zero even components for the cores of 30 elliptical galaxies. Such components could arise as a result of a non-equilibrium state of the core, but in this case it should be random whether a blueshift or a redshift would result. S&S's measurements showed a redshift in 27 out of 30 cores, which would be statistically very unlikely if the shift was a result of random non-equilibrium movement. On the other hand the measurements could be explained, if part of the even components were due to gravitational redshift. S&S calculated an expected maximum value of about 20 km/s for the gravitational redshift velocity of a galaxy in their sample.

- In 1995 Alberto Cappi [8] attempted to capture the effect in a sample of cD-clusters. He measured the velocity difference ΔV between the cD and the mean velocity of the cluster. This difference is largely due to peculiar motion in the cluster and ΔV can therefore have both signs.

  The contributions to ΔV coming from peculiar motion, can be expected to even out if one considers the mean of the ΔV's $\langle \Delta V \rangle$ for a large number of clusters, so only the part of ΔV resulting from gravitational

redshift will remain. Cappi used this procedure on a sample of 41 clusters, all with a minimum of 25 measured redshifts. For the total sample he found a negative value of $\langle \Delta V \rangle$ and the same was the case when a subsample of 22 galaxies with $\sigma \leq 750$ km/s was considered separately. But the complementary subsample of 19 clusters with $\sigma >$ 750km/s exhibited a positive $\langle \Delta V \rangle$ although with a large uncertainty. Since the effect of gravitational redshift scales with mass, it is to be expected that high mass clusters will be the easiest place to detect the effect. Still the sample used by Cappi was to small to allow a conclusive detection of the gravitational redshift effect.

- In 2002 Broadhurst and Scannapieco (b&S) [6] consider two different possibilities for measuring the effect

    1. The possibility of using the redshift of line emission from the metal rich intercluster medium, as a probe of gravitational redshift in the cluster. To estimate the magnitude of the effect, the emission weighted mean potential along the line of sight was calculated, based on the density distribution of an isothermal sphere. For a cluster with $\sigma = 1200$ km/s the velocity resulting from the gravitational redshift was predicted to have a value of about 50 km/s at a radius of 100 kpc/h.
    2. They also considered a sample of 8 massive clusters each containing a cD-galaxy and all with velocity dispersion above 700 km/s. For this sample they found that all but one cluster had cDs exhibiting a redshift relative to the mean cluster velocity. Summing over all the relative cD velocities $\sum \Delta V_{cD}$ and weighting this sum by the variance, they found an average value of $\langle \Delta V_{cD} \rangle = 260 \pm 58$ km/s.

- In 2004 Kim and Croft [17] rejected the possibility of measuring the effect with the data available, based on an examination of a sample of simulated clusters made by a N-body simulation. From the simulated clusters they found the gravitational velocity difference between the central and the outer parts of the potential to be of the order of 10 km/s, for a cluster mass of $M \sim 10^{15} h^{-1} \mathrm{M}_{\odot}$, and that a detection on a 2σ level would require at least 2500 cluster with masses $M > 10^{13} h^{-1} \mathrm{M}_{\odot}$. Since such a number of clusters with sufficient redshift data is not

available, they concluded that a detection of the effect is not within reach.

The above summary does by no means give a clear and unambiguous answer to question of the possibility of measuring the effect of gravitational redshift in clusters of galaxies. It does however point out several possible ways to approach the problem, some of which I will discuss in the following

1.3 The possible approaches

The results cited above suggest a number of different possible approaches to the problem of measuring the gravitational redshift in galaxy clusters:

1. If a number of massive cluster with a large number of redshifts is available, it might be within reach to measure the effect in the individual clusters. This could be done by looking at the redshift difference between the mean values for galaxies residing in the centre and the mean of galaxies in the outskirts. This possibility would of course depend on that the mass distribution had a high central concentration. If the effect was of a magnitude comparable to the highest values cited above - i.e. $\simeq 150$ km/s in a cluster with a total mass of about $5.0\times10^{15}h^{-1}\mathrm{M}_{\odot}$ and a velocity dispersion of about 1500 km/s, a simple calculation shows that an inner and an outer sample of about 400 redshifts would be needed to obtain a 2σ detection of the effect. For a slightly lighter cluster with mass $1.0 \times 10^{15}h^{-1}\mathrm{M}_{\odot}$ and velocity dispersion of about 1000 km/s the expected effect found by Cappi is around 40 km/s. A 2σ detection would therefore demand about 2500 redshifts in each of the two samples. The problem with this approach is that there are quite few of the very massive clusters in the observable universe and that knowledge of the mass distributions in these does not necessarily translate into a more general understanding of the mass distribution in the more common clusters of intermediate and low mass.

2. Another option would be to consider a sample of clusters all having a centrally dominant BCG, and then from these form a composite cluster consisting of all the galaxies in the sample. The galaxy redshifts used in this cluster would be the redshifts of each galaxy relative to the redshift of it's respective BCG. The composite cluster could then be divided into a number of shells and the mean values over the redshifts of

the galaxies in each shell could be determined. If each shell contained a sufficient number of galaxies, the velocity contributions from random movement should tend to even out and the velocity contribution from gravitational redshift should the be visible as a variation in the mean out through the cluster. The massive galaxy in the centre would increase the steepness of the central potential, which in turn would boost the effect of gravitational redshift. If the dominant central galaxy could be considered to be relatively at rest in the dark matter potential it would also lessen the noise level from peculiar velocities, so the effect could be more easily measured. Since the velocity dispersions of clusters are supposed to depend strongly on mass, this can be done without scaling of the individual clusters, if only clusters in a relatively narrow velocity dispersion range were considered.

3. A third possibility would be to use a larger number of clusters with differing velocity dispersions also possessing a central galaxy and then form a composite cluster as described above. In this case, since the effect would vary significantly with cluster mass, it would necessary to perform a scaling of positions and velocities for each cluster.

1.4 Thesis outline

In this thesis I will attempt to use the second and third approach on three different samples of galaxy clusters. I will compare the result obtained from these, with estimates from both analytical calculations and from two simulated galaxy clusters.

In the following I will give a short outline of the contents of the chapters in the thesis.

- In the first chapter I have given an introduction to the theory underlying the phenomena of gravitational redshift. Then I have described previous efforts to detect the effect and have finally outlined a possible way to proceed towards a measurement.

- Chapter 2 estimates the gravitational redshift effect determined analytically based on two different density distributions.

- Chapter 3 describes the cosmological simulation that has been used

and presents the gravitational redshift velocity profiles resulting from the simulated clusters.

- In chapter 4 the three data samples are presented and the methods used for cluster member selection and scaling are described.
- Chapter 5 contains the results of the attempts to measure gravitational redshift in the composite clusters, created for each of the three samples of clusters.
- Chapter 6 attempts to explore whether it is realistic to expect the central BCGs in a cluster to be more or less at rest with respect to the mean velocity of the rest of the cluster galaxies.
- Chapter 7 summarises an discusses the results from the previous chapters.

Chapter 2

Analytical estimates of the effect

A possible way of estimating the effect of the gravitational redshift in a cluster of a given mass, is to assume a density profile and use this to calculate the gravitational potential Φ as a function of radius. From this the gravitational redshift z_g can easily be determined. By finding the value at the centre of the potential and assuming that the effect is very close to zero at the outskirts of the cluster, the expected size of the effect can be estimated.

2.1 The Hernquist profile

A possible choice of density profile is the de Vaucouleurs profile, which has been observed to give a reasonable good fit to regular clusters. This profile is given by the following expression

$$\Sigma(R) \quad = \quad \Sigma_e \exp(-7.67[(\frac{R}{R_e})^{\frac{1}{4}} - 1]) \tag{2.1}$$

where R is the projected radius, R_e is the effective radius of the isophote enclosing half the light and Σ_e is the projected density at R_e.

The density distribution given by the de Vaucouleurs law has a characteristic cusp in the central density that could be consistent with the enhancement in density caused by the presence of a centrally dominant galaxy. For this reason, the potential deduced from this distribution, might be relevant in making an estimate of the expected effect of gravitational redshift, in galaxy clusters with massive central galaxies.

Hernquist [13] proposed a density distribution, which is a close approximation to a deprojected version of the de Vaucouleurs law. The Hernquist distribution is given by the following expression:

$$\rho(r) = \frac{Ma}{2\pi r}\frac{1}{(r+a)^3} \tag{2.2}$$

where M is the total mass and a is a scale length, related to R_e by the expression $a = \frac{R_e}{1.8153}$ [8].
Integration of the density expression produces the following form of the potential

$$\phi(r) = -\frac{GM}{r+a} \tag{2.3}$$

where r is the distance from the centre. To get an approximate value for the total mass of a cluster with a given R_e and a given velocity dispersion, I have followed the lead of Cappi [8] and used the Poveda formula given by

$$M = 9\frac{R_e\sigma^2}{G} \tag{2.4}$$

as an expression for the total mass of a cluster with a Hernquist distribution. From this it follows that the gravitational velocity V_g can be expressed as

$$V_g(r) = -\frac{\phi(r)}{c} \tag{2.5}$$

$$= \frac{GM}{c(r+a)} \tag{2.6}$$

$$= \frac{9R_e\sigma^2}{c(r+a)} \tag{2.7}$$

and from this the expected gravitational redshift difference defined as

$$\Delta V_g(r) = V_g(0) - V_g(r) \tag{2.8}$$

can be plotted for a cluster with a given velocity dispersion, with R_e as the only free parameter. The result of this for two clusters with velocity dispersions of 500 km/s and 1000 km/s respectively, are shown in figure 2.1 and 2.2 for two different values of R_e. The value of R_e for a given value of σ was found by considering the relation between σ and R_e described in chapter 4.

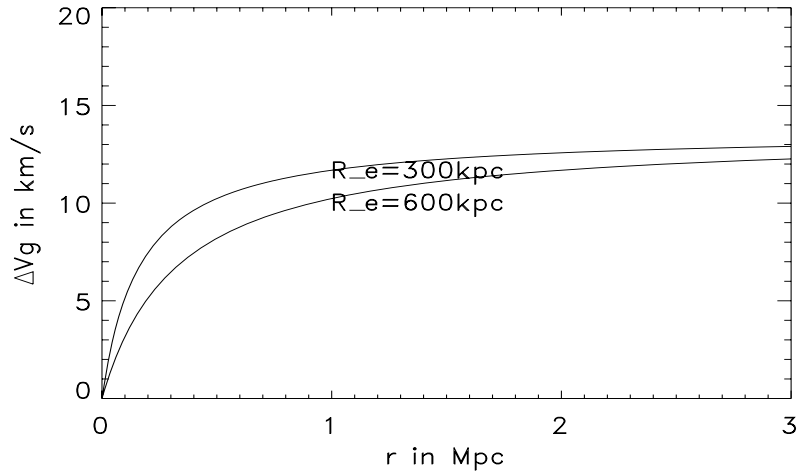

Figure 2.1: The gravitational velocity as a function of distance from centre for a cluster $\sigma = 500\mathrm{km/s}$ *and for two different values of the half-light radius* R_e

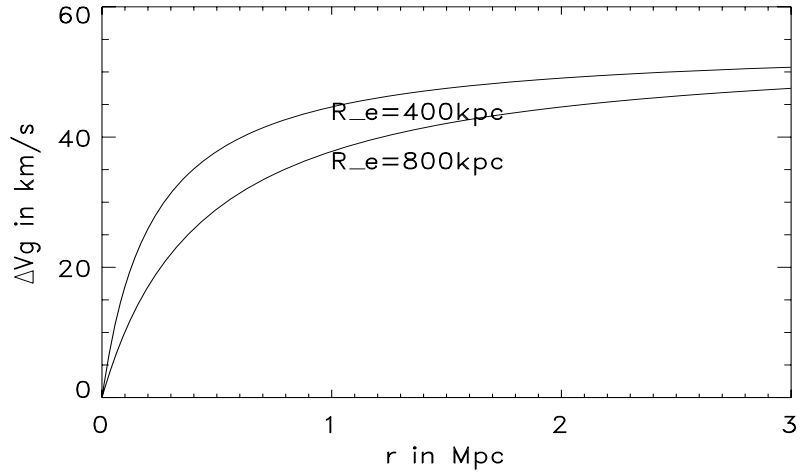

Figure 2.2: The gravitational velocity as a function of distance from centre for a cluster $\sigma = 1000\mathrm{km/s}$ *and for two different values of the half-light radius* R_e

The plots show a value of $\Delta V_g(R_{max})$ of about 50 km/s and 13 km/s for the massive cluster and the less massive cluster respectively.

If composite clusters are formed how many individual clusters would then be needed if a 2σ detection of the effect of gravitational redshift should be possible? Assuming that the uncertainty is given by the expression

$$\delta = \frac{\sigma}{\sqrt{N}} \tag{2.9}$$

where N is the number of galaxies in the cluster, then from the condition for a 2σ detection

$$\delta_{max} = \frac{\Delta V_g}{2} \tag{2.10}$$

where δ_{max} is the maximum allowed error for a 2σ detection, it follows that

$$\delta_{max,\sigma=500} \simeq 7\text{km/s} \tag{2.11}$$

and

$$\delta_{max,\sigma=1000} \simeq 25\text{km/s} \tag{2.12}$$

and from this it follows that the number of galaxies needed to make a 2σ detection is given as

$$N_{gal,\sigma=500} = \frac{(500\text{km/s})^2}{(7\text{km/s})^2} \tag{2.13}$$

$$\simeq 6000 \tag{2.14}$$

and

$$N_{gal,\sigma=1000} = \frac{(1000\text{km/s})^2}{(25\text{km/s})^2} \tag{2.15}$$

$$\simeq 1600 \tag{2.16}$$

If clusters with a minimum of 50 redshifts are available, it would then take 120 clusters to make a 2σ detection for clusters with $\sigma = 500$ km/s and 32 cluster for clusters with $\sigma = 1000$ km/s. This is under the assumption that there are no significant contributions to the noise, apart from the random movement of the cluster galaxies.

The cited numbers should be obtainable (see the section on the available number of clusters), so if the prediction given by the Hernquist distribution gives an accurate estimate, it should be possible to measure the effect of gravitational redshift in clusters of galaxies.

2.2 The NFW-profile

Another possible density profile is given by the NFW-distribution defined by Navarro, Frenk and White [18]. This distribution has been shown to give a very good fit to dark matter halos produced in cosmological simulations based on a CDM scenario. The NFW distribution is now also widely used to describe the mass distribution of observed galaxy clusters.

The distribution depends on two parameters, the concentration parameter c and a scale radius r_s, which in turn is related to the radius r_{200}, where the density is 200 times the critical density, by the expression $c = \frac{r_{200}}{r_s}$. The NFW density expression has the following form

$$\rho(r) = \frac{\rho_{crit}\delta_c}{\frac{r}{r_s}(1+\frac{r}{r_s})^2} \tag{2.17}$$

where δ_c is related to the concentration parameter c by the expression

$$\delta_c = \frac{200}{3}\frac{c^3}{\ln(1+c) - \frac{c}{1+c}} \tag{2.18}$$

And where ρ_{crit} is the critical density.

The potential resulting from this distribution is calculated in the appendix and is given by

$$\phi(r) = -\frac{4\pi G\rho_{crit}\delta_c r_s^3}{(r_s+R_t)}\left(1 + \frac{(r_s+R_t)\ln\left(\frac{r_s}{r+r_s}\right)}{r}\right) \tag{2.19}$$

where R_t is a cut-off radius for the distribution.
The central value (see appendix) is given by the expression

$$\phi_0 = \frac{4\pi G(\rho_{crit}+\delta_c)r_s^2 R_t}{(r_s+R_t)} \tag{2.20}$$

In order to compare the gravitational redshift profile deduced from this distribution with other analytical profiles, the results from simulation and from observation, it is convenient to relate the distribution to the cluster velocity dispersion. Girardi et al. [11] considers a sample of 170 nearby ($z \leq 0.15$) cluster and find the following approximate relation between the virial radius and the projected velocity dispersion σ_p

$$r_{vir} \simeq 0.002\sigma_p(h^{-1}\mathrm{Mpc}) \tag{2.21}$$

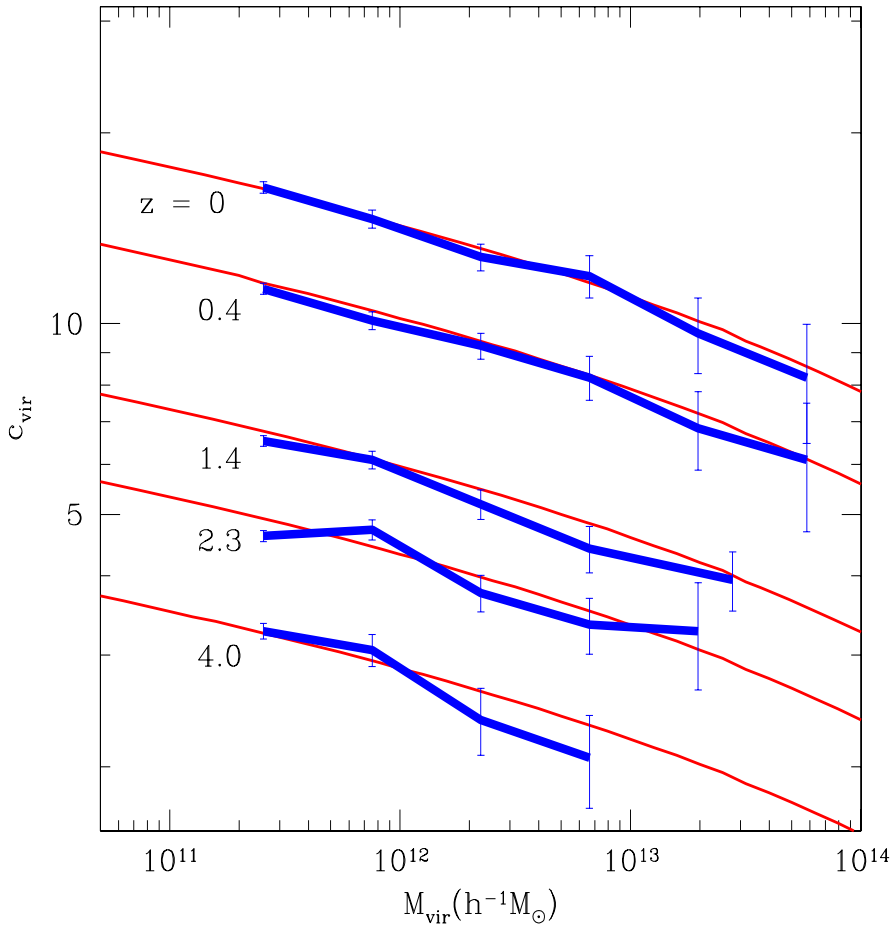

Figure 2.3: Median values of c_{vir} as a function of M_{vir} for haloes at five different redshifts. The figure is taken from Bullock et al. [7]

By taking $r_{200} \simeq r_{vir}$ and then using the approximate relation of Girardi et al. and the relation between c, r_{200} and r_s, the gravitational velocity difference of a NFW distribution can be plotted for a cluster with a given σ and a given cut-off radius R_t and with the concentration parameter c as the only free parameter. The choice of the value of the concentration parameter c for a given value of σ has been based on the work of Bullock et al. [7]. They investigate the halo concentration of a sample of 5000 dark matter haloes in the matter range $10^{11} - 10^{14} h^{-1}\mathrm{M}_{\odot}$ from a N-body simulation based on a

ΛCDM cosmology.
The result of this study is shown in figure 2.3. If the trend seen in the figure can be extrapolated to more massive haloes, it seems that a value around to $c = 5$ would be reasonable choice for the concentration parameter of a massive galaxy cluster with a velocity dispersion around 1000 km/s, whereas a slightly higher value of about $c = 8$, should be expected for a less massive cluster with a dispersion around 500 km/s. Here the connection between cluster mass and cluster velocity dispersion is based on the work of Popesso et al. [24] reviewed in the end of this section.

The result of the NFW distribution for clusters with $(\sigma, R_t) = (500, 2)$ and $(\sigma, R_t) = (1000, 3)$ respectively, are shown in figure 2.4 and 2.5. The

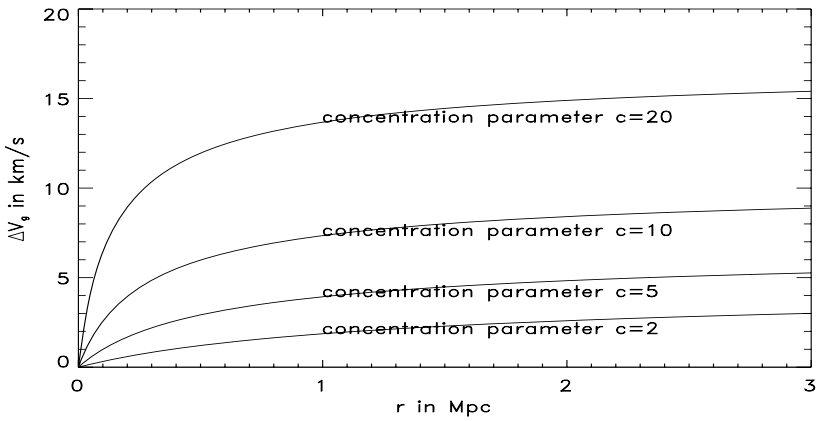

Figure 2.4: The gravitational velocity as a function of distance from centre for a cluster $\sigma = 500$km/s *and for four different values of the concentration parameter c*

plots give the following values of $\Delta V_g(R_{max})$. For a cluster with $\sigma \simeq 500$km/s, $\Delta V_g(R_{max})$ can be expected to be found in the range of $3 - 15$ km/s, with a most likely value around 8 km/s and for a more massive cluster with $\sigma \simeq 1000$ km/s, $\Delta V_g(R_{max})$ should be in the range $10 - 55$ km/s, with a most likely value around 20 km/s. These values are somewhat lower, than the values deduced from the Hernquist distribution and this seems reasonable, since the central density cusp in the Hernquist distribution can be expected to boost the effect of gravitational redshift in the cluster.

From the values cite above and still assuming a minimum of 50 redshift pr.

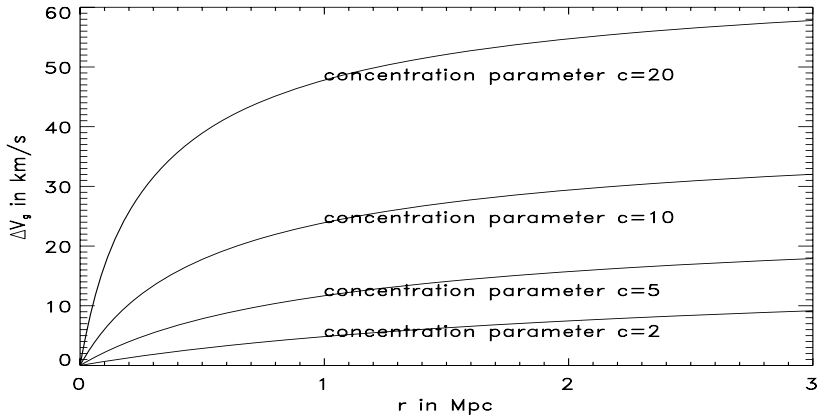

Figure 2.5: The gravitational velocity as a function of distance from centre for a cluster $\sigma = 1000$km/s *and for four different values of the concentration parameter c*

cluster, the number of clusters needed would be around 300 for $\sigma = 500$ km/s and 200 for $\sigma = 1000$ km/s. These numbers might be fairly high especially with regard to the massive clusters. Assuming a larger number of redshifts per cluster, which is not unreasonable considering the recent improvements in observing techniques, would bring down the number of clusters needed and a detection might therefore still be within reach.

2.3 The number of available clusters

A pertinent question in regard to measurement of the effect of gravitational redshift is whether there are a sufficient number of clusters available in the observable universe.

Bahcall and Bode [2] studied the relationship between the numbers of clusters with mass greater than $8 \times 10^{14} h^{-1} \mathrm{M}_{\odot}$ pr cubic Mpc and the linear amplitude of the mass fluctuations σ_8. Their results are shown in figure 2.6, where the lines are given by analytic predictions, whereas the points are result of an N-body simulation.

Kim and Croft[17] fits a power law to the points in the figure and finds the following expression for the number of clusters n with $M > 8 \times 10^{14} h^{-1} \mathrm{M}_{\odot}$

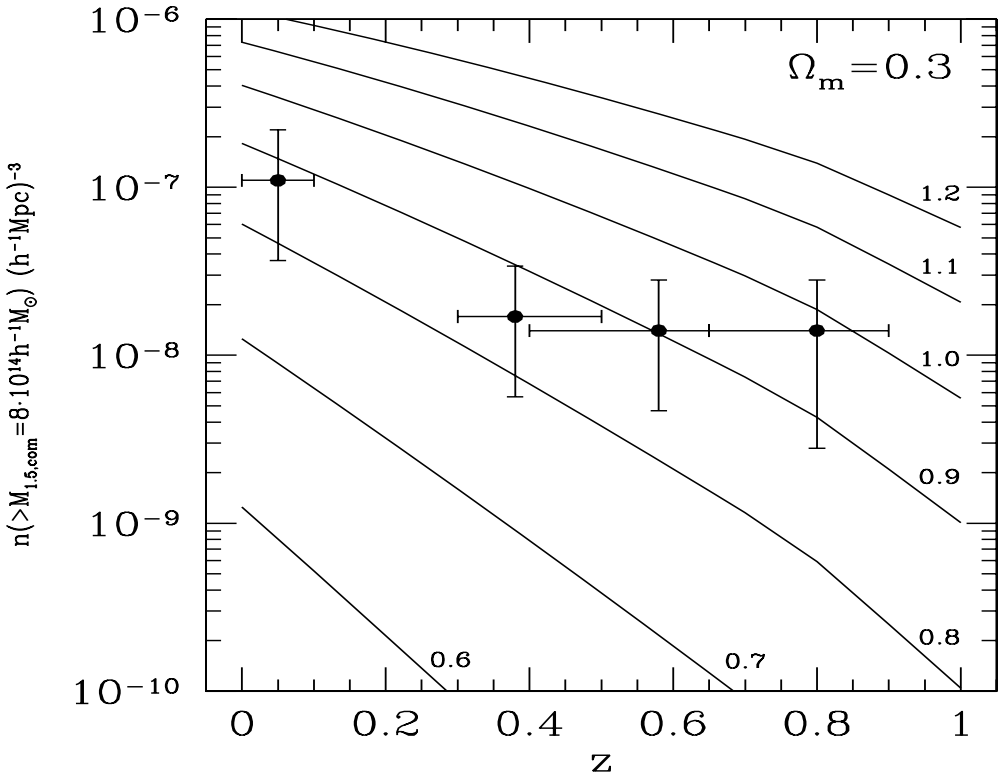

Figure 2.6: Evolution of cluster abundance with redshift, for different values of σ_8. The figure is taken from Bahcall and Bode[2]

pr cubic Mpc, as a function of z.

$$log(n) \simeq 2z - 6.75 \tag{2.22}$$

With the aid of the comoving distance function given by

$$D = D_H \int_0^z \frac{dz'}{E(z')} \tag{2.23}$$

where

$$E(z) = \sqrt{\Omega_M(1+z)^3 + \Omega_K(1+z)^2 + \Omega_\Lambda} \tag{2.24}$$

and $D_H = 3000h^{-1}$Mpc and $\Omega_M = 0.3$ and $\Omega_\Lambda = 0.7$, the total number of clusters with $M > 8 \times 10^{14}h^{-1}\mathrm{M}_\odot$ with $z \leq 1$ can be expressed as

$$N = 4\pi D_H^3 \times 10^{-6.75} \int_0^1 \frac{10^{-2z}}{E(z)} \left[\int_0^z \frac{dz'}{E(z')} \right] dz \qquad (2.25)$$

From numerical integration of this expression, they find that there are about 600 clusters with $M > 8 \times 10^{14}h^{-1}\mathrm{M}_\odot$ available in within $z \leq 1$.

To relate the number of available clusters with masses $M > 8\times10^{14}h^{-1}\mathrm{M}_\odot$ to the estimates of the gravitational redshift in galaxy clusters of different velocity dispersion made in this section, the correspondence between cluster mass and cluster velocity dispersion has to be estimated. For this purpose I have considered the following two relations found by Popesso et al. [24].

The first relation is between the total optical luminosity and the mass inside r_{500} and the second between the velocity dispersion and the mass inside r_{500}. The total optical luminosity and the velocity dispersions are measured quantities, whereas the mass inside r_{500} is calculated from the virial theorem based on the positions and velocities of the cluster galaxies and if necessary extrapolated beyond these using a NFW density profile. Plots of the two relations are displayed in figure 2.7 and 2.8.

From combined considerations of the relations displayed in the two figures I find that a lower mass limit of $M = 8 \times 10^{14}h^{-1}\mathrm{M}_\odot$ correlates roughly to a lower limit in cluster velocity dispersion of approximately 1000 km/s, though the rather large scatter in the relations makes it difficult to determine a more exact value. If this correspondence in the lower limits of mass and velocity dispersion of clusters is about right and if the estimate of the number of available clusters made by Kim and Croft [17] is reasonable, it follows that there are about 600 clusters with velocity dispersions $\sigma \geq 1000$ km/s. If the estimates of the effect of gravitational redshift in galaxy clusters made in this section are valid, this number of clusters should be sufficient to facilitate a detection of the effect.

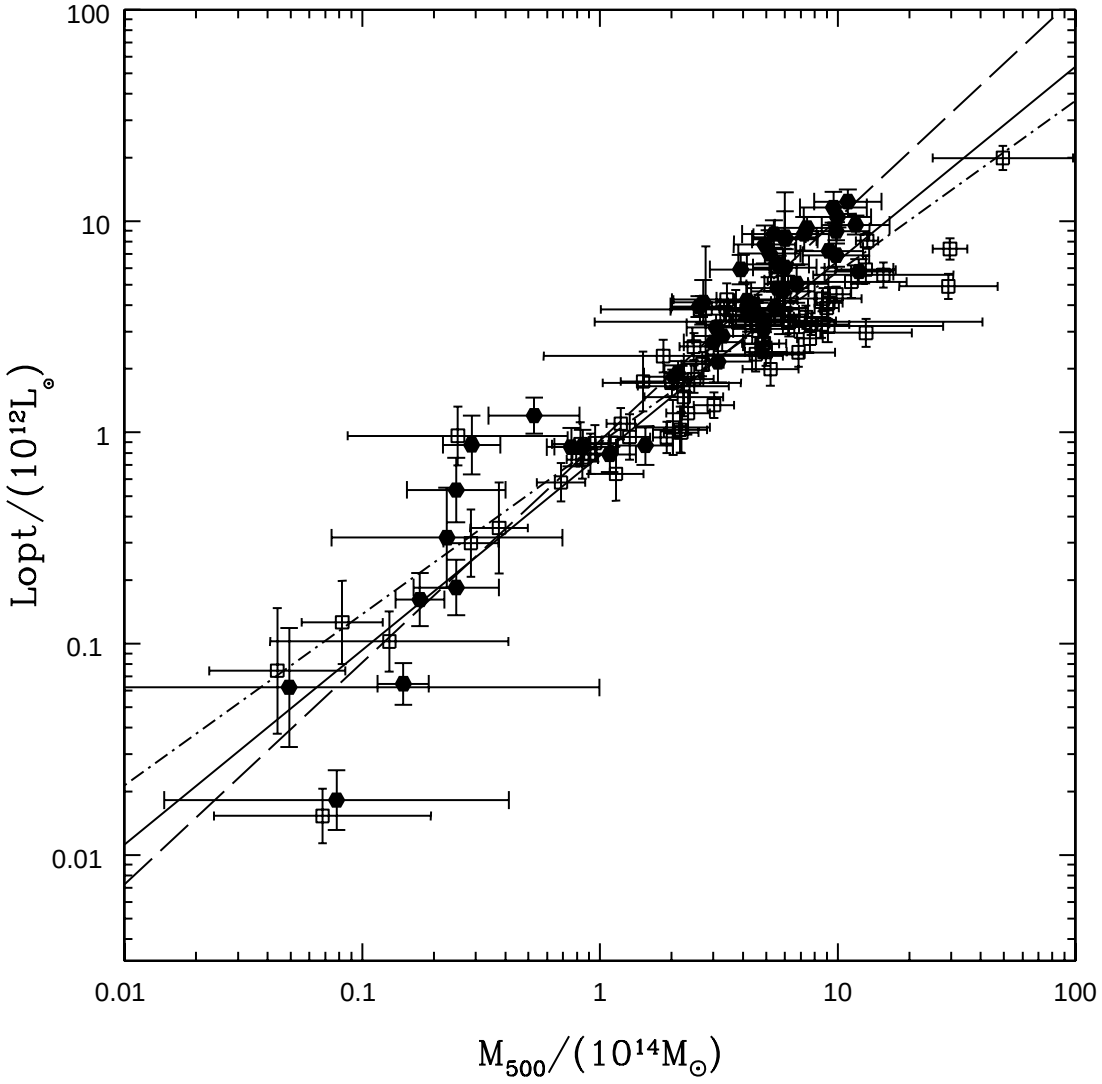

Figure 2.7: Optical luminosity versus mass inside r_{500} for 102 *clusters of the RASS-SDSS cluster survey. All systems have mass estimates made through virial analysis. Filled dots indicate systems for which mass estimates have also been made with the aid of the relation between x-ray temperature and mass. The figure is taken from Popesso et al [24]*

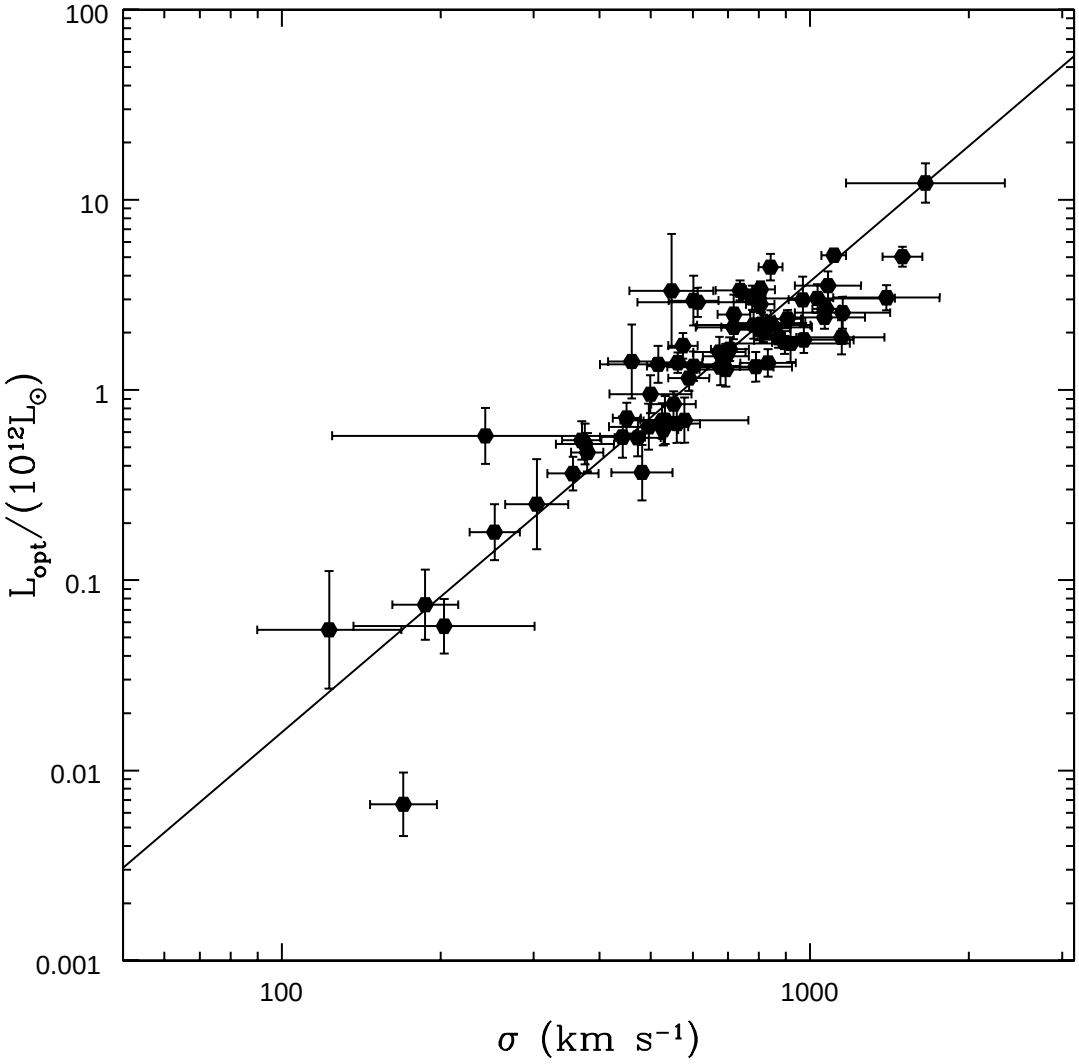

Figure 2.8: Optical luminosity versus mass inside r500 for 114 clusters of the RASS-SDSS cluster survey. The figure is taken from Popesso et al [24]

Chapter 3

The simulations

3.1 The simulation method

The simulated clusters used in this thesis originate from a cosmological (ΛCDM) TREESPH simulation. The TREESPH-code is a combination of two techniques that allow incorporation of gas dynamical processes together with an effective calculation of the gravitational acceleration of the individual particles. The method consist of the following two parts:

- SPH - Smoothed particle hydrodynamics: In SPH the gas dynamical processes in astrophysical systems are modelled by considering a fluid consisting of an infinite number of infinitesimal fluid elements. The state of a fluid can be described by its density ρ, its pressure p and its velocity field v. These are related through the continuity equation

$$\frac{\partial \rho}{\partial t} = \bigtriangledown \cdot (\rho \mathbf{v}) = 0 \tag{3.1}$$

  Euler's equation

$$\frac{\delta \mathbf{v}}{\delta t} + (\mathbf{v} \cdot \bigtriangledown)\mathbf{v} = -\frac{1}{\rho}\bigtriangledown p - \rho \bigtriangledown \Phi \tag{3.2}$$

  and the equation of state

$$p = p(\rho) \tag{3.3}$$

  where Φ is the gravitational potential.

SPH is based on an interpolation method which makes it possible to express a given field, in terms of its values at a set of points. With the aid of a differentiable kernel W, a differentiable interpolant of the field can be constructed. The interpolation points are obtained by selecting a sample of fluid elements and letting each selected element be represented by of simulation particle. Since only a small percentage of the fluid elements is represented by particles it is necessary to introduce a smoothing procedure. This is done by letting the kernel W depend on a smoothing length h that can correct local statistical fluctuations in the particle number. Instead of perceiving the particle as localized at a point, it can be visualized as being smeared out around its actual location, with a distribution given by W and a "smear-radius" given by h. The density at a given point r can the be calculated by summing the contributions from particles, which contains the point inside the "smear-radius" h, so that a mean density at the point r can be expressed as

$$\langle \rho(\mathbf{r}) \rangle = \sum_{i=1}^{N} m_i W(\mathbf{r} - \mathbf{r}_i; h) \tag{3.4}$$

Where m_i is the mass of the i'te particle.

The size of a given contribution from particle i will depend on the distance from r to the particles actual location r_i, on the shape of W, and on the size of h. Any physical field depending on density, will then also depend on the choice of W and h. The smoothing function W will generally resemble a delta function for $h \to 0$ and only particles within $2h$ of the actual position will be included in the smoothed field. One effect of the smoothing procedure is that the scale of the local spatial resolution will be determined by h. The number of particles inside $2h$ of a point will decide the accuracy of the smoothed field, so that more precise estimates are obtained for higher particle densities. To obtain the same accuracy everywhere and at the same time increase the resolution at areas of high density (which will in general be the most interesting places), it is common to let the smoothing length be spatially variable. Since the variation of density often will evolve with time, it is also common to let h be time dependent.

- TREE - the hierarchical tree method: This is a technique used for computing the gravitational interaction between the simulation particles.

The calculation of the gravitational force on a particle i is done by organizing the rest of the particles in a nested hierarchy according to distance, having a tree form with the largest structures at the top. The tree is constructed by recursively subdividing the volume of the simulation into regular cubic cells. The leaves of the tree will then consist of the cells containing only one particle.

The method of choice for calculating the interaction between particle i and a given particle j among the rest, will depend on the position of j in the tree-structure made for i. Forces from nearby particles are calculated as direct particle-particle interactions, which is a precise, but not very efficient method for a large number of particles $\tilde{\mathrm{O}}(N^2)$. The influences from the more remote particles are included by considering multipole expansions of clusters (of particles) - i.e. the precise distribution of particles inside the cluster is ignored and only the overall shape of the cluster counts. Since the number of particles in a clusters generally will be vastly greater than the number of terms in the multipole expansion for the cluster, this method will increase the efficiency of the calculation.

The method will include an accuracy criterion, which determines the maximum size of an unresolved cluster at a given distance.

When calculating the force on a particle, the routine starts at the top of the tree and the contributions from each part of the tree is summed as they are passed to the tree.

In TREESPH the routines from SPH and the hierarchical tree method is combined to perform a cosmological simulation, including gas dynamics. With set of initial conditions specified for a chosen initial value of the redshift z, the routines of TREESPH is performed at each time step and the time are stepped forward using a leapfrog integrator.

3.1.1 Group finding

The first step in the analysis of the result of a TreeSPH simulation of a galaxy cluster, is to identify the groups of particles that can be interpreted as member galaxies of the cluster. For the simulations referred to here the identifying procedure went as follows: The clusters of the simulations are selected by visual inspection and for each cluster the following procedure is

then performed to determine the final member galaxies of the cluster. In the z=0 frame, the cluster is overlaid with a cubic grid with cube length $\Delta l = 10$ kpc. Each cube is inspected and the number of star particles inside is counted and cubes with $N_{star} \geq 2$ are selected. A larger cube with cube length $3\Delta l$ is then centred on each of the selected cubes. If the larger cube contains at least 7 gravitationally bound star particles, it is identified as a possible galaxy candidate. Since a star particle often will be assigned to more than one galaxy candidate, the candidate with the greatest number of star particles is selected among the candidates having star particles in common. The resulting set of galaxies is taken to be the member galaxies of the cluster.

3.2 Results from simulations

I have used simulated clusters resulting from simulations performed by Sommer-Larsen et al. [29, 26, 30, 31]. These simulations are made by taking a selection of dark matter halos obtained from a pure dark matter cosmological N-body simulation with a cosmological scenario given by a standard flat ΛCDM model ($h = 0.7, \Omega_0 = 0.3, \Omega_b = 0.036, \sigma_8 = 0.9$) and a box length of $L = 150h^{-1}$Mpc. The Halos are then resimulated using a TreeSPH code. In the resimulation baryonic particles to represent stars and gas, are added to the DM particles of the original simulation. Particle numbers are in the range 100000-500000 SPH+DM particles and the particle masses for gas, stars and DM have the values $m_{Gas} = m_{star} = 3.1 \times 10^7 h^{-1}\mathrm{M}_\odot, \mathrm{m_{DM}} = 2.3 \times 8\mathrm{h}^{-1}\mathrm{M}_\odot$. From the results of two runs of the simulation from z=13.5 to z=0, the two clusters C1 ($\simeq$ 3keV) and C2($\simeq$ 6keV) are selected. Both of these clusters contain a central cD-galaxy in their z=0 frame.

The two simulated clusters can be used to estimate the values of the size of the gravitational redshift effect for the two different cluster masses, they can give information on the movement of the cDs relative to the cluster centre of mass and on the dispersions of the velocities of the cluster galaxies.

The velocity offset of the cDs relative to the total centre of mass including dark matter is found to be 33 km/s and 207 km/s for C1 and C2 respectively. When the velocities of the BCGs are considered relative to the mean value of the velocities of the cluster galaxies the velocity offset between BCG and mean has a magnitude of 186 km/s and 248 km/s for C1 and C2 respectively. These values are in good agreement with the value of around $100 - 300$ km/s found for the majority of cDs in a number of surveys (see chapter 6). The

difference in the two velocity offsets for C1 shows that even when a central galaxy is close to being at rest relative to the total centre of mass and thereby relative to the centre of the potential this does not necessarily translate into the galaxy being nearly at rest relative to the mean velocity of the cluster galaxies.

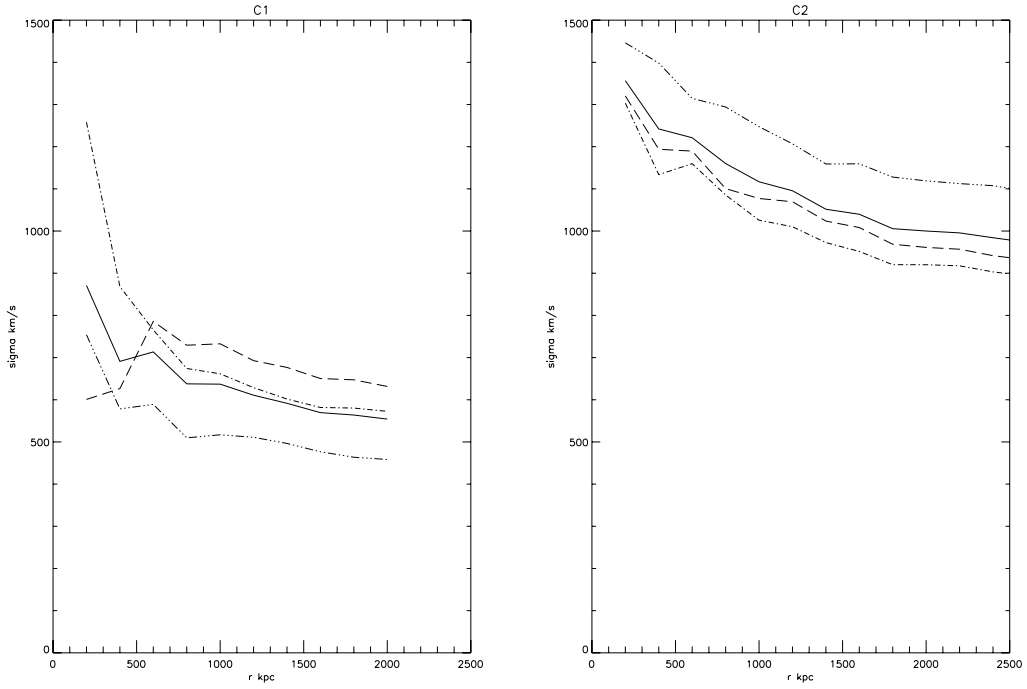

(a) Velocity dispersions for C1. Dashed lines are 1-dim. dispersion along x, y and z-axis. The solid line is the mean value of the three 1-dim dispersions

(b) Velocity dispersions for C2. as for C1.

Figure 3.1:

In order to determine how the velocity dispersion corresponds to the expected effect for the two simulated clusters, I have plotted the velocity dispersion as a function of radius for the three velocity coordinates v_x, v_y and v_z. These are shown in figure 3.1. Since the error in the mean of the measured (projected) velocity in a given data will depend on the projected velocity

dispersion this is of primary interest in evaluating the size and number of redshifts of the sample of a given type of clusters needed to make a significant detection of the effect of gravitational redshift. The projected dispersion is taken as the mean of the projected dispersion arising when looking at the cluster along the three coordinate axes.

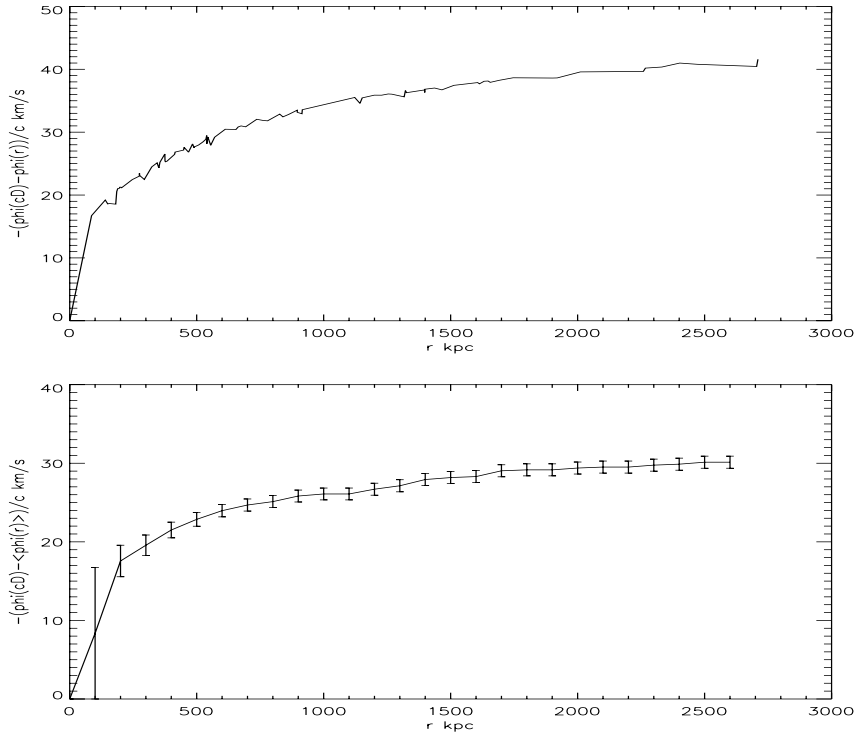

Figure 3.2: The gravitational redshift velocity as a function of distance from centre (CM of galaxies) for the C2 cluster

In order to estimate the size of the effect of gravitational redshift in the two simulated clusters the gravitational redshift velocity profile is plotted for both clusters. The profile for the two simulated clusters is depicted in figure 3.2 and 3.3

The plots show how ΔV given as

$$\Delta V(r) = -\frac{\Delta\phi}{c} \tag{3.5}$$

$$= -\frac{(\phi(cD) - \phi(r))}{c} \tag{3.6}$$

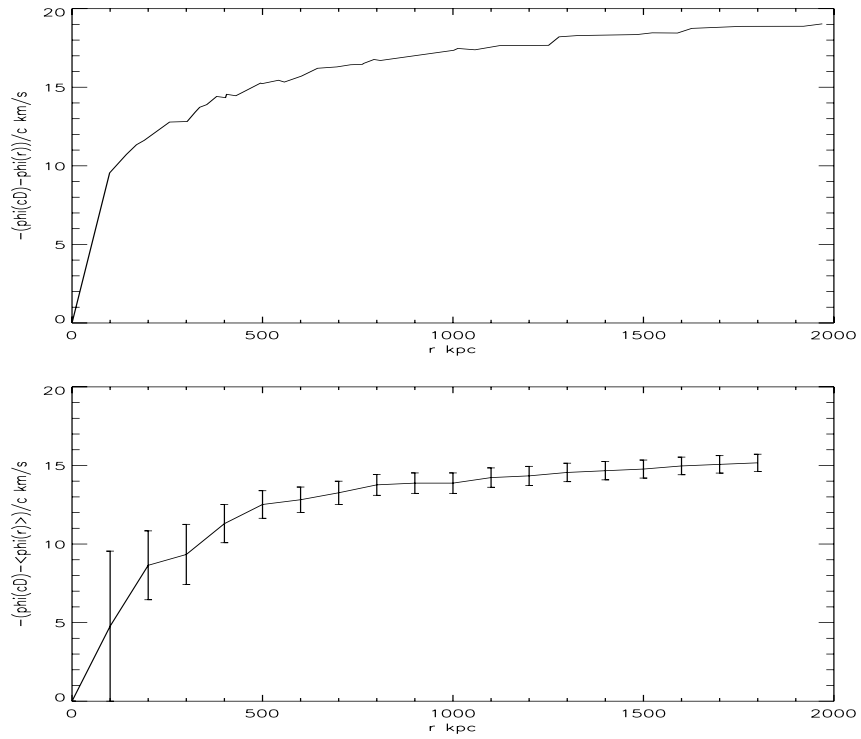

Figure 3.3: The gravitational redshift velocity as a function of distance from centre (CM of galaxies) for the C1 cluster

varies out through the two simulated clusters. In the top plot the variation of $\Delta V(r)$ with radius is displayed, whereas the bottom plot shows the variation of $< \Delta V(r) >$ given as

$$\Delta V(r) = -\frac{\Delta\phi}{c} \tag{3.7}$$

$$= -\frac{(\phi(cD) - \langle\phi(r)\rangle)}{c} \tag{3.8}$$

where the mean is taken over all galaxies inside r.

For a cluster with $\sigma \simeq 500$ km/s (C1) the simulations predict an effect of the order of 18 km/s and a 2σ detection would therefore require an uncertainty below 9 km/s and for a cluster with $\sigma \simeq 1000$ km/s (C2) the simulations predict an effect of about 40 km/s and a 2σ detection would require an uncertainty below 20 km/s. From calculations similar to the ones

done in chapter 2.1, it follows that the number of galaxies needed for a 2σ detection is

$$N_{gal,C1} = \frac{(500\text{km/s})^2}{(9\text{km/s})^2} \tag{3.9}$$

$$\simeq 3000 \tag{3.10}$$

for the lower mass cluster C1 and

$$N_{gal,C2} = \frac{(1000\text{km/s})^2}{(20\text{km/s})^2} \tag{3.11}$$

$$\simeq 2500 \tag{3.12}$$

for the more massive cluster C2. If clusters with a minimum of 50 redshift were available, this would be equivalent to 60 and 50 clusters of the C1 and C2 type respectively.

Chapter 4

The data and the method of data selection

4.1 The data samples

4.1.1 The RASS-SDSS

The RASS-SDSS survey constructed by Popesso et Al [23], [24], consists of 114 clusters (and groups) with position inside the area of the sky covered by the Sloan Digital sky survey (SDSS) and inside the mass range of $10^{12.5}M_{\odot} \leq M \leq 10^{15}M_{\odot}$ and the redshift range $0.002 \leq z \leq 0.45$. The aim of the study behind this survey is to construct a database of clusters that contain both x-ray and optical data in the form of Schechter luminosity function parameter, bolometric luminosity, core density, core radius, total radius and half-light radius for all members. This will allow a study of the correlation between x-ray and optical properties for clusters.

The criteria for the selection of clusters are, apart from what is mentioned above, that they should be x-ray clusters and that they must be observed by SDSS. The X-ray observations are selected from the following ROSAT based surveys:

- The ROSAT-ESO flux limited x-ray survey (Reflex) $0.1-2.4$ keV down to a limiting flux of $3 \times 10^{-12}\text{erg}^{-1}\text{cm}^{-2}$ consisting of 448 clusters.

- The northern ROSAT all-sky survey cluster sample (NORAS) $0.1-2.4$ keV with a flux limit of $2 \times 10^{-12}\text{erg}^{-1}\text{cm}^{-2}$ with about 1300

clusters.

- The ASCA cluster catalogue (ACC) contains 273 clusters and groups.
- The group sample (GS) which contains 66 systems with $\sigma < 600$km/s.

The RASS-SDSS contain all x-ray systems from the sources mentioned above, which lies inside the area covered by SDSS until Sep. 2003.

The selection of the galaxy sample belonging to a given cluster is performed as described in section 4.2 and the total luminosity of the cluster is calculated on the basis of the magnitudes of all galaxies in the sample. Using a maximum likelihood method a King profile given as

$$P(r) = \frac{\sigma_0}{\left(1+\left(\frac{r}{r_c}\right)^2\right)^{\beta}} + \sigma_b \tag{4.1}$$

is fitted to the observed spatial distribution of galaxies in each cluster, where σ_0 is the central galaxy density, with a value obtained from the normalisation condition

$$\int_A P(r) d(\pi r^2) = N_{tot} \tag{4.2}$$

for the total cluster area A. r_c, β and σ_b are the core radius, the profile exponent and the background density respectively, and are all treated as fitting parameters. From the King profile, the physical size of the cluster r_{tot} is estimated as the radius where the galaxy number density has fallen to 3 times the error of the background galaxy density. The half-light radius is now determined as follows: The total optical luminosity of the cluster in a given band, is presumed to be the luminosity in this band calculated inside r_{tot} and the total luminosity is then the sum over the luminosities in each band. The luminosity in each of the four bands is estimated stepwise, from the centre and out to r_{tot} and the radius within which the sum is equal to half the total value is determined.

By using the galaxy selection procedure described in section 4.2 on data from the SDSS archive, I have attempted to reconstruct the RASS-SDSS sample. The primary advantage of this sample is that it can be considered complete in the sense that all X-ray detected clusters in the area covered has been included.

4.1.2 The Abell samples

The Abell samples consists of well-studied Abell clusters with a large number of redshifts and a central BCG. These are found by checking the literature to find the names of the most studied clusters and then perform a near name search in NED for each cluster name, in order to find an initial sample of galaxies for each cluster. The galaxy selection procedure described in section 4.2 of this chapter is then used on these initial samples.

The sample consists of two subsamples with the following characteristics: The first subsample contains clusters with a minimum of 50 member galaxies, redshift less than 0.1 and velocity dispersion between 750 km/s and 1250 km/s.

The second subsample consists of clusters with a minimum of 50 members, redshifts less than 0.1 and velocity dispersions between 250 km/s and 750 km/s.

The aim of these two samples is to have a selection of cluster where the central BCGs have been previously studied in the literature. This will increase the likelihood that the BCGs are actual members of their respective host clusters and not just field galaxies or galaxies from other clusters seen in projection. All clusters in the samples either have a BCG classified as a cD or a D galaxy or have a BCG recorded in the Postman [25] catalogue of BCGs. The reason for limiting the samples to clusters with a large number of redshifts is to obtain a higher certainty for the value of the cluster velocity dispersion. This is of importance with respect to the assumption of correspondence between cluster velocity dispersion and cluster mass. The downside to these samples is that they can in no respect be considered complete and that they might therefore be inflicted with unrealised biases.

4.2 Member galaxy selection

For all the three samples the selection of member galaxies, have been done by the method of Hartog and Katgert [12] described in the following.

Defining the centre of the cluster To classify galaxies as either members of the cluster or projected galaxies from the field or from other clusters, one needs to refer to the cluster centre/ the minimum of the cluster potential. It is therefore necessary to have a rather clear notion of the position of this.

Since the gas in clusters is expected to settle in the potential on a reasonably short timescale, hot x-ray emitting gas is likely give a good indication of the position of the cluster potential minimum. Because the intensity of the emitted x-ray radiation is proportional to the electron density squared, it will also generally trace the regions of the highest density of baryonic matter. Since the RASS-SDSS is based on a selection of x-ray detected clusters, central coordinates based on x-ray observations, are available for all the clusters survey and these will be employed in the following as indicators of cluster centres.

For the Abell samples centre cluster coordinates from NED have been applied as the position of the cluster centre.

The aim of the member selection procedure is to include as cluster members all the galaxies inside turnaround radius. The selection is done in a number of steps.

In the first step an initial sample of galaxies for a given cluster, is selected from the archive by taking all galaxies within an Abell radius from the cluster centre having a redshift z satisfying that $|cz - cz_{cluster}| \leq 4000$ km/s, where $z_{cluster}$ is the mean cluster redshift given in the x-ray catalogues. Since there is no clear definition of the mean cluster redshift $z_{cluster}$ recorded in the x-ray catalogue, I am hesitant to make extended use of this quantity, but since some preliminary redshift/velocity criteria is needed to determine an initial sample, it has been necessary to use it in some cases. For clusters with a known central BCG, the redshift of this has been used instead of the mean cluster redshift. In clusters not having a previously known BCG, the mean cluster redshift from the x-ray catalogue has been used only in the first step of the member galaxy selection procedure.

All galaxies in the initial sample are plotted in a redshift histogram and galaxies exhibiting a weighted gap in velocity space relative to the adjacent galaxies , which is greater than 4, are rejected as a member of the cluster. For the order statistics of a sample, the gaps in the distribution is defined as:
$g_i = v_{i+1} - v_i, \quad i = 1, \ldots, n-1$
where the i's give the order in velocity space. The gaps are weighted according to their place in the velocity distribution with weights given as
$w_i = i(n-i)$.

After rejection the remaining galaxies are then used to determine a upper and lower bound for the allowed velocity of the sample. A new archive search is performed with the determined velocity constraints and a maximum radius of 3 Abell radii and the second step of the selection procedure is applied to

the sample resulting from this search.

It is not simple to decide whether an individual galaxy has or has not turned around. Partly because massive clusters have velocity dispersion that can exceed 1000 km/s and therefore galaxies have to be rather far from the centre ($r \geq 20$Mpc) for their Hubble expansion velocity relative to the cluster to be sufficiently large as to set them apart significantly from the cluster. Furthermore this problem is increased by the fact that the gravitational pull of the cluster will affect the expansion of the close surroundings. However in most cases a decrease in velocity dispersion as a function of radius is observed and this will improve the situation. Katgert et Al assume a spherical symmetric mass distribution and apply the virial theorem to find an estimate of the mass profile for the cluster. This profile is then utilized to find the maximal radial velocity that a galaxy inside turnaround radius can have. This is done by considering the following model of the cluster. The cluster is viewed as being spherically symmetric and consisting of a central region, which is relaxed and which has an isotropic velocity distribution. The inner region has radius r_{vir} and surrounding this region is a region of infall with radius r_{turn}. From the virial theorem $K = -\frac{1}{2}W$ the following expression can be deduced as an estimate of the mass inside a given radius

$$M(r) \simeq M_{VT} \quad = \quad \frac{3\pi N}{2G} \frac{\sum_i (V_i - \overline{V})^2}{\sum_{j>i} \frac{1}{R_{ij}}} \tag{4.3}$$

Where r is the distance to the cluster centre, R is the projection of r, N is the number of galaxies in the sample placed inside R, V is the line of sight velocity and R_{ij} is the projected distance between galaxy pairs ij. In the infall region between r_{vir} and r_{turn} the virial theorem is not valid, but the mass estimate made with the above expression can be used as an upper limit to the mass inside r_{turn}. From this a mass profile (or an upper limit to one) follows for the entire cluster. This enables the calculation of the circular velocity v_{circ} at a given radius, that a galaxy would have if it where on a purely circular orbit. In the infall region the galaxies will be on bound ingoing orbits, i.e. $K \leq W$ and this means that the infall velocity is limited upwards as $v^2_{infall} \leq 2v^2_{circ}$.

The following three criteria is now applied to each galaxy in the possible sample to check its member status:

1. The whole cluster is considered to be in infall and galaxies are assumed to be either on radial orbits toward the centre or on purely circular

orbits. In the first case the observed velocities at projected distance R will have an upper limit given by the maximum value of the line-of-sight component of $v(r)_{infall}$ for $r \leq r_{turn}$. In the later case the maximum velocity will be given as the maximum component of the circular velocity in the direction of line-of-sight. The maximal allowed velocity as a function of projected radius R is then given by

$$\begin{aligned} V_{max}(R) &= max(v_{infall}(r)cos\theta, v_{cir}(r)sin\theta) && (4.4) \\ &= max(2v_{cir}(r)cos\theta, v_{cir}(r)sin\theta) && (4.5) \end{aligned}$$

where θ is the angle between $\mathbf{r}$ and the line-of-sight, which will pick-out the relevant components, and the second equation follow from the assumption of the whole cluster being in infall.

2. The second criterion is equal to the first for galaxies with projected positions between r_{vir} and r_{turn}. For galaxies seen as projected inside of r_{vir} the velocity distribution is expected to be isotropic and the orbits can have any orientation. Therefore the maximum possible value of the velocity that can be observed at projected radius R, is not dependent on the angel between $\mathbf{r}$ and the line-of-sight, so $V_{max}(R) = v_{infall}(r)$, when $R \leq r_{vir}$.

3. The third criterion assumes an isotropic velocity distribution in the whole cluster inside $r = r_{turn}$ and $V_{max}(R)$ is therefore given as $V_{max}(R) = v_{infall}(r)$.

All galaxies with velocity values $|v| > |v_{max}|$ in all the three criteria are then removed from the sample. The method is used iteratively, by recalculation of the mass profile after each round of removals. The final sample will then contain the galaxies left when the mass profile has reach its converging value. Convergence is found to be reached in one to ten iterations.

The procedure described above requires a minimum of 45 galaxies in the sample at the start of the iteration. For samples with less than this number, the removal of interlopers is done by the following statistical method: For the sample of clusters with more than 45 galaxies initially, Hartog and Katgert [14] finds that clusters members (of the final samples) and interlopers are relatively well separated in the (R/r_{200},$|v - \langle v \rangle|/\sigma_p$) plan, where $\langle v \rangle$ and σ is the mean velocity and the velocity dispersion for the initial sample of the second step. They are therefore able to define a separating demarcation

line between members and interlopers in this plane. This demarcation line can then serve as a tool to spot interlopers in the samples with less than 45 members, when these are plotted in the (R/r_{200},$|v - \langle v \rangle|/\sigma_p$) plane.

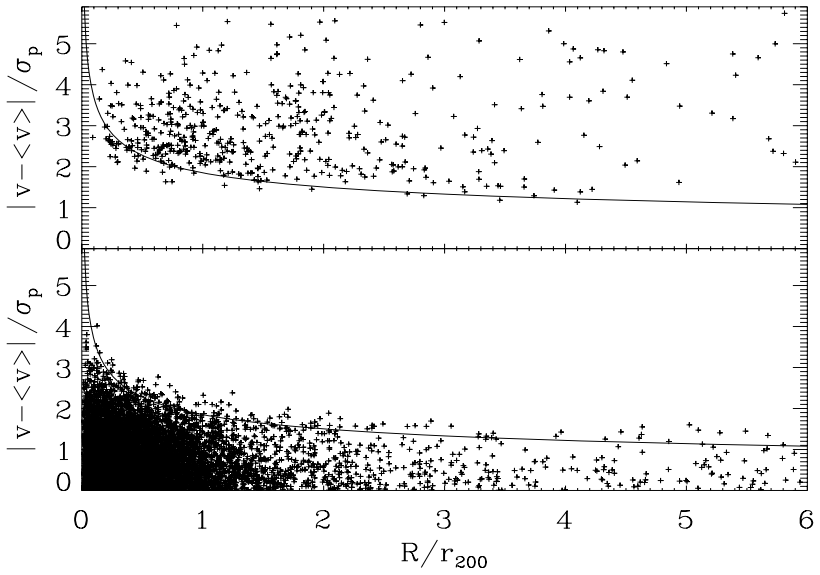

Figure 4.1: The demarcation line in the ($\frac{r}{r_{1000}}$, $\frac{|v-\langle v \rangle|}{\sigma}$)-plane, separating interlopers (above), from members (below). The figure is taken from Hartog and Katgert [14]

Figure 4.1 shows the demarcation line found by Hartog and Katgert. For cluster with less than 45 redshift this demarcation line are employed to separated interlopers from members. Since one of the cluster samples used in this thesis, has several cluster members with less than 45 members it has been necessary to employ the demarcation method here. I have therefore created a plot similar to the one made by Hartog and Katgert, based on all the clusters in the two main samples the Abell sample and the RASS-SDSS sample. To avoid heavy extrapolation of the mass profile determined in step two, the galaxies is plotted in the ($\frac{R}{r_{1000}}$, $\frac{|v-\langle v \rangle|}{\sigma}$) space instead of the ($\frac{R}{r_{200}}$, $\frac{|v-\langle v \rangle|}{\sigma}$) space as in Hartog and Katgerts plot.

Figure 4.2 shows the demarcation line found by using all clusters with

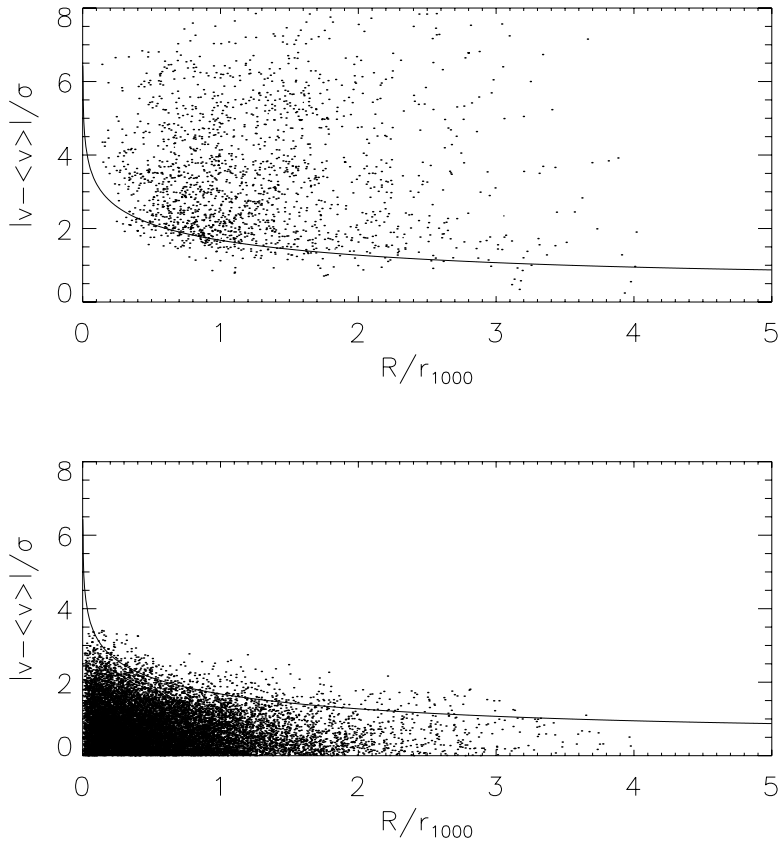

Figure 4.2: 1800 interlopers (above) and 18210 member galaxies (below), from 110 clusters taken from the RASS-SDSS sample and the Abell sample.

45 or more galaxies in the initial sample, from both the RASS-SDSS sample and the Abell sample. The chosen demarcation line is given by the following expression

$$y = -0.7\ln(x) + 0.08x + 1.6 \tag{4.6}$$

The member selection for all clusters with less than 45 redshifts in the initial sample was performed this with the aid of this demarcation line.

In summary the member galaxies in the RASS-SDSS cluster sample constructed by Popesso et al are selected in the following manner: The galaxies

are selected among objects in SDSS categorised as galaxies. The centre of the cluster is defined as the centre of the observed x-ray Source. The selection is done in two steps:

1. In the first step galaxies that satisfy the following criteria are selected:

   (a) The galaxies should lie within a radius of 2.15 Mpc of the centre of their host cluster.

   (b) Their velocity relative to the mean cluster velocity, should be less than 4000 km/s -
   $|cz - cz_{cluster}| < 4000$ km/s.

   The weighted gaps are calculated for order statistics in velocity space and objects that exhibits weighted gaps $g_i w_i \geq 4$ in the velocity distribution, are rejected from the sample, whereby the limits of the cluster in velocity space are defined.

2. A new sample with velocities inside the interval defined in the preceding step and with a greater radius cut-off is now selected from the SDSS database. On this sample the method of Katgert et al. is then applied to weed out interlopers.

By this method Popesso et al. [23] and [24] arrive at a sample of 114 clusters with at least 10 members each.

4.2.1 Scaling of the RASS-SDSS sample

The gravitational redshift depends strongly on mass and thereby on σ. Furthermore the maximum radius within which redshifts are available for a Given cluster will influence the magnitude of the measured velocity difference between the centre and the outer parts of the cluster. When constructing a composite cluster from a sample of clusters with a wide spectrum of velocity dispersions and cut-off radius, it is therefore necessary to perform a scaling according to velocity and radius, so that all positions and velocities of all galaxies in the composite cluster are scaled according to a common standard.

The velocity scaling can be done by defining a standard cluster, as a cluster having velocity dispersion $\sigma = \sigma_{standard}$. When a sample of n clusters are combined to form a composite cluster, the velocities from the individual

clusters are scaled by multiplying all velocities in i'te cluster with the factor v_{scale} given as

$$v_{scale} = \frac{\sigma_{standard}}{\sigma_i} \tag{4.7}$$

where σ_i is the velocity dispersion of the i'te cluster.
To make a scaling according to radius, some characteristic radius has to be known for all clusters in the cluster sample. As mentioned in section 4.1.1 both the core radius consistent with a King profile and the half-light radius have been determined for most of the clusters in the RASS-SDSS sample by Popesso et al.

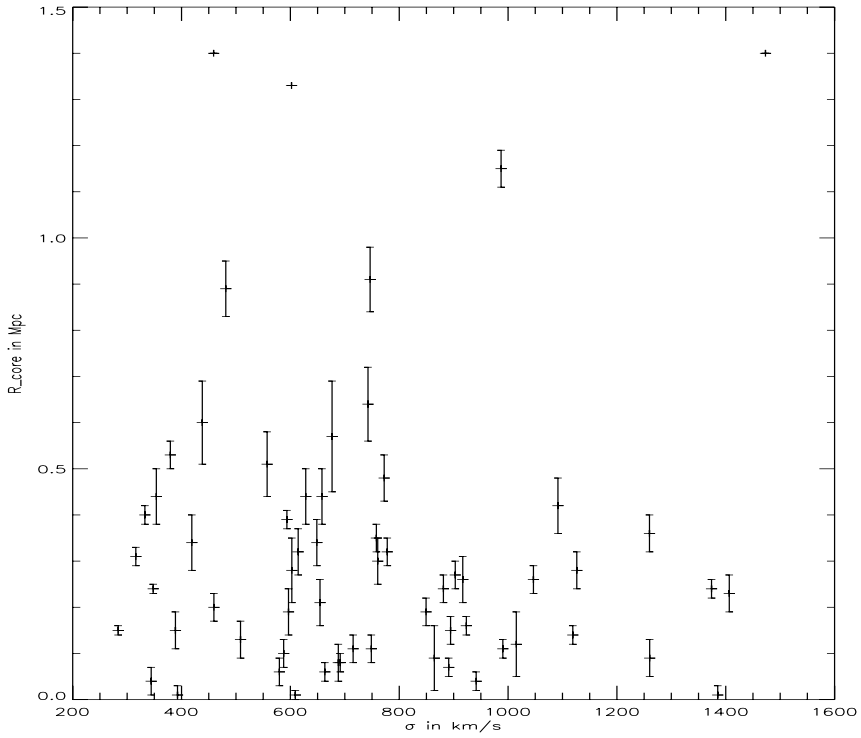

Figure 4.3: Velocity dispersion inside R_{1000} versus core radius for 78 clusters from the RASS-SDSS cluster sample

In order to perform a scaling of the galaxies in each of the clusters according to position, I've investigated the relation between

1. Half-light radius $R_e$versus velocity dispersion of galaxies inside R_{1000}.

2. Core radius R_c of the King profile versus velocity dispersion of galaxies inside R_{1000}.

To insure reasonable good statistics only clusters having at least 20 galaxies inside R_{1000} have been included in the following plots.

In figure 4.3 displays a plot of velocity dispersion versus core radius for 78 from the RASS-SDSS. From the figure it becomes clear, that there are no apparent correlation between the core radius for the fitted King profile of the cluster and the cluster velocity dispersion of the galaxies within R_{1000}. The core radius therefore does not seem like a sensible choice as characteristic radius for a scaling of the clusters.

In figure 4.4 the relation between the half-light radius R_e and the cluster velocity dispersion of the galaxies within R_{1000} is depicted. Here a correlation seems to exist and figure 4.5 shows two possible fits to the $\sigma - R_e$ relation. The functions $R_{e,1}$ and $R_{e,2}$ are given by the following expressions

$$R_{e,1}(\sigma) = 0.000409954\sigma + 0.117998 \quad (4.8)$$

$$R_{e,2}(\sigma) = 0.0870083\sigma^{0.354425} - 0.474403 \quad (4.9)$$

The size of the uncertainties of R_e in figure 4.4, makes it impossible to compare the goodness of the fits in detail and there is therefore no base for choosing one above the other of the two fits. In the following I have used the first fit function $R_{e,1}(\sigma)$, which from now on I will simply refer to as $R_e(\sigma)$.

The scaling according to radius is then executed by multiplying the radial positions of all galaxies in the i'te cluster with the factor

$$R_{scale} = \frac{R_e(\sigma_i)}{R_e(\sigma_{standard})} \quad (4.10)$$

As a standard cluster I have chosen a cluster with a velocity dispersion of $\sigma_{standard} = 500$ km/s. The reason for this choice is that I would like to be able to compare my results to the results from one of the simulated clusters. Since the $\sigma - R_e$ relation used for the scaling has the most data points in the low to intermediate velocity dispersion range, a standard cluster of the same velocity dispersion as the C1 simulated cluster seemed to be the most sensible choice.

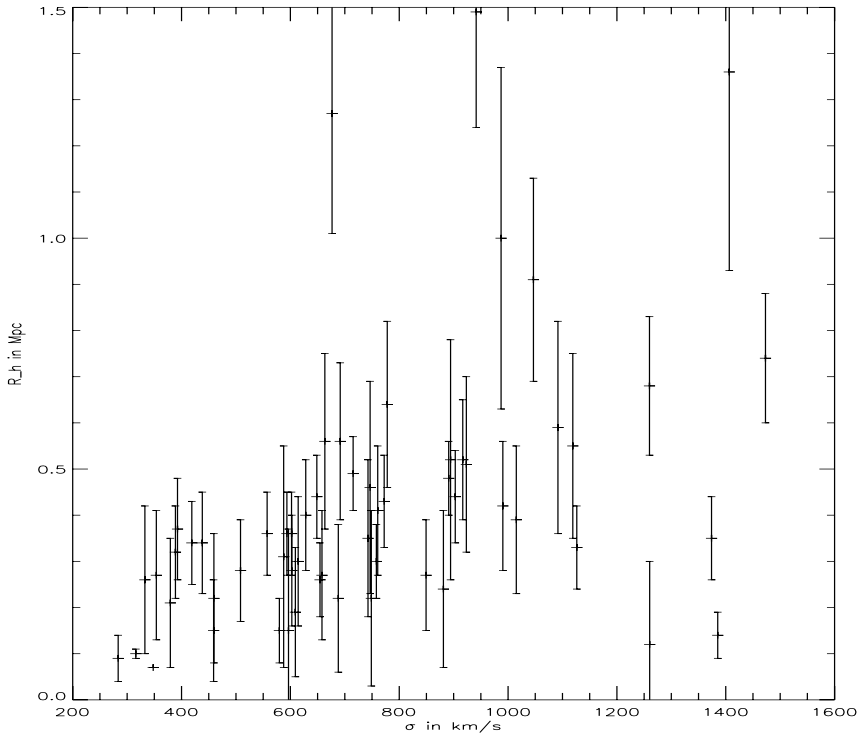

Figure 4.4: Velocity dispersion inside R_{1000} versus half-light radius for 78 clusters from the RASS-SDSS cluster sample

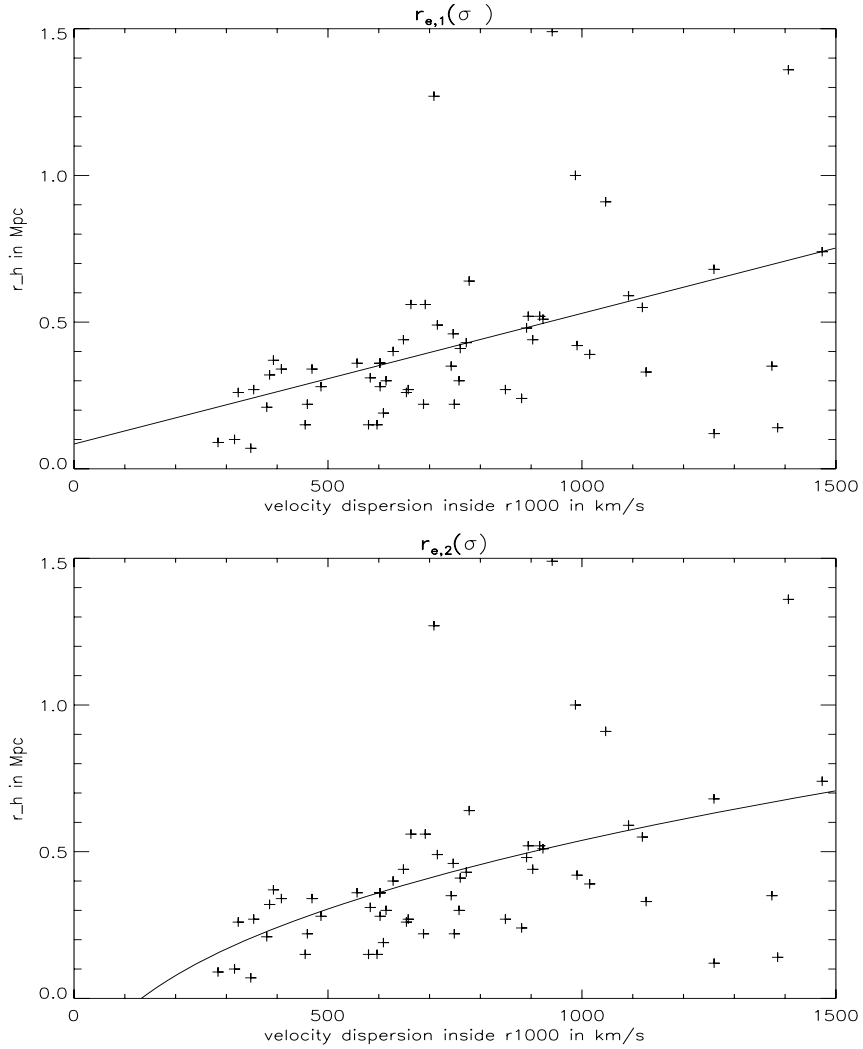

Figure 4.5: Two possible fits to the $R_e - \sigma$ relation

Chapter 5

Results

In the following attempt to detect gravitational redshift it is assumed that the movement of the cluster galaxies relative to the central BCG can be considered to consist of pure random movement. If this is the case the mean of the relative velocities of a large sample of cluster galaxies should primarily be the velocity resulting from gravitational redshift, since the contributions from random movement will tend to even out if a large enough number of redshifts are available. As a result of this assumption the only uncertainties included in the plots in this chapter will be the uncertainties resulting from the random movements of the cluster galaxies.

The assumption of pure randomness for the movement of the cluster galaxies is generally not considered to be accurate. Substructure resulting from recent merger events in the cluster, might cause different systematic movements in different parts of the cluster. Furthermore the movements of both the central galaxy and some or all of the cluster members, might be influenced by systematic movements of the dark matter in the cluster. As an example of this, in the C2 cluster of the simulation, the inner cusp of the dark matter distribution exhibits a strong rotational movement (Sommer-Larsen, private communications). Even though these effects might influence the possibility of measuring the gravitational redshift in a single cluster, it could be expected that the systematic velocity contributions will even out, when a composite cluster is constructed from a sufficiently large number of individual clusters with different systematic movements.

With the aid of the selection procedures described in the preceding chapter, a sample of member galaxies have been chosen for each cluster in the three cluster samples. The data in these samples consists of the redshift,

two position coordinates relative to the cluster centre, the magnitude in the r-band for each of the galaxies, the number of members in each cluster and the centre position for each cluster.

In order to select clusters with a central BCG and use these to form a composite cluster for each of the cluster samples, the following ssteps are performed for all three cluster samples

1. The brightest galaxy is selected from each cluster. If this BCG lies within 0.1 Mpc of the cluster centre it is defined as a "central BCG", and the cluster is selected as a participant of the composite cluster. This creates a subsample for each of the three main cluster samples, consisting of all the clusters in the samples having a "central BCG". All further work will be done on these subsamples.

2. In order to correct for the different cosmological redshifts of the different clusters, the velocity of the "central BCG" in a given cluster is subtracted from all other galaxies in this cluster. The corrected velocity $v_{cor,i}$ of the i'te galaxy in the j'te cluster can be expressed as

$$v_{cor,i} = v_i - v_{BCG,j} \tag{5.1}$$

   the correction made in this step relies on that assumption that the BCG can be considered to be at rest (or very close to) in the center of the potential.

3. The velocity dispersion σ_{cor} of the v_{cor}'s of all galaxies in each cluster is now calculated.

4. If a scaling is required the procedure described in section 4.2 is followed. The σ_{cor}'s for each cluster are used to determine a $R_e(\sigma_{cor})$ for the cluster. If a scaling is performed the scaled positions and velocities will be the ones used in the following steps.

5. All galaxies belonging to clusters with a "central BCG" is now combined in a composite cluster. Three composite clusters are thus created. One for the RASS-SDSS cluster sample (figure 5.1) and one for each of the two subsamples of the Abell Sample (figure 5.8 and figure 5.9).

6. The mean velocity of the galaxies in the composite cluster as a function of radius is now calculated in two ways

(a) The cluster is divided into i shells each containing k galaxies. For each shell the mean value of the velocities of its k galaxies is calculated as

$$v_{mean}(shell_i) = \frac{1}{k}\sum_{j=1}^{k} v_{j,cor} \tag{5.2}$$

To each shell corresponds a radius $R(shell_i)$, which delimits the outer boundary of the shell. The inner boundary is given by the radius of the previous shell $R(shell_{i-1})$. Since the shells are made to contain the same number of galaxies they are not even spaced. For each shell the standard error of the mean is also calculated. The reason for the above calculation of the mean values is to gain information of the variation of the mean velocity of the composite cluster as a function of radius.

(b) The cluster is considered stepwise in m steps according to increasing radius, so each step i corresponds to a radius R_i and so that $R_i = R_{i-1} + \Delta R$ where ΔR is a fixed step size. The mean value of the velocities of the all the $n(i)$ galaxies within R_i is then calculated as

$$v_{mean,i} = \frac{1}{n(i)}\sum_{j=1}^{n(i)} v_{j,cor} \tag{5.3}$$

This gives the variation in the mean velocity of the cluster as galaxies further and further out is included. Since the mean calculated in a given step will not be independent of value calculated in the previous steps, it is clear that the main point in the calculation will be the mean value of all the galaxies in the composite cluster given as

$$v_{mean,total} = \frac{1}{n}\sum_{j=1}^{n} v_{j,cor} \tag{5.4}$$

where n is the total number of galaxies. The reason for this second way of calculating the mean, is to get values which include a large number of galaxies, thereby reducing the uncertainties.

7. In step two I defined the corrected velocities of the galaxies in the composite cluster, as the velocities relative to their respective BCGs. The idea of detecting the effect of gravitational redshift by looking at the mean values computed in step six, relies on the assumption that on average the velocities of the galaxies can be expected to be lower than that of their BCG. This should follow from the fact that the magnitude of the gravitational redshift will be greatest in the centre of the cluster where the BCG is located. Therefore one would expect to see the following three general trends

   - Negative mean values of the corrected velocities computed in step six.
   - A mean close to zero in the central area of the cluster
   - An increase in the (negative) magnitude of the mean with radius.

   To visualize the variation of the mean velocity of the composite cluster as a function of radius I have made the two following plots for each of the three composite clusters.

   (a) A plot A of the pairs $(R(shell_i), -v_{mean}(shell_i))$, with $i = 1, 2, 3, 4$.

   (b) A plot B of the pairs $(R_i, -v_{mean,i})$ with a step size of $\Delta R = 0.05$Mpc.

   In order to compare with the predictions from analytical calculations made in section 2.1 and 2.2 and the simulation results from section 3.2 I have preferred to visualize the mean velocity variation with radius for the composite cluster, as a positive quantity. Therefore the mean values are given a negative sign in the above description of the mean velocity versus radius plots.

In the following sections I will describe the results of the member selections for the three main cluster samples and consider the plots resulting from the steps outlined in the above.

5.1 The RASS-SDSS

From the 114 cluster in the RASS-SDSS sample the cluster selection procedure finds 78 clusters with more than 20 member galaxies. These 78 clusters

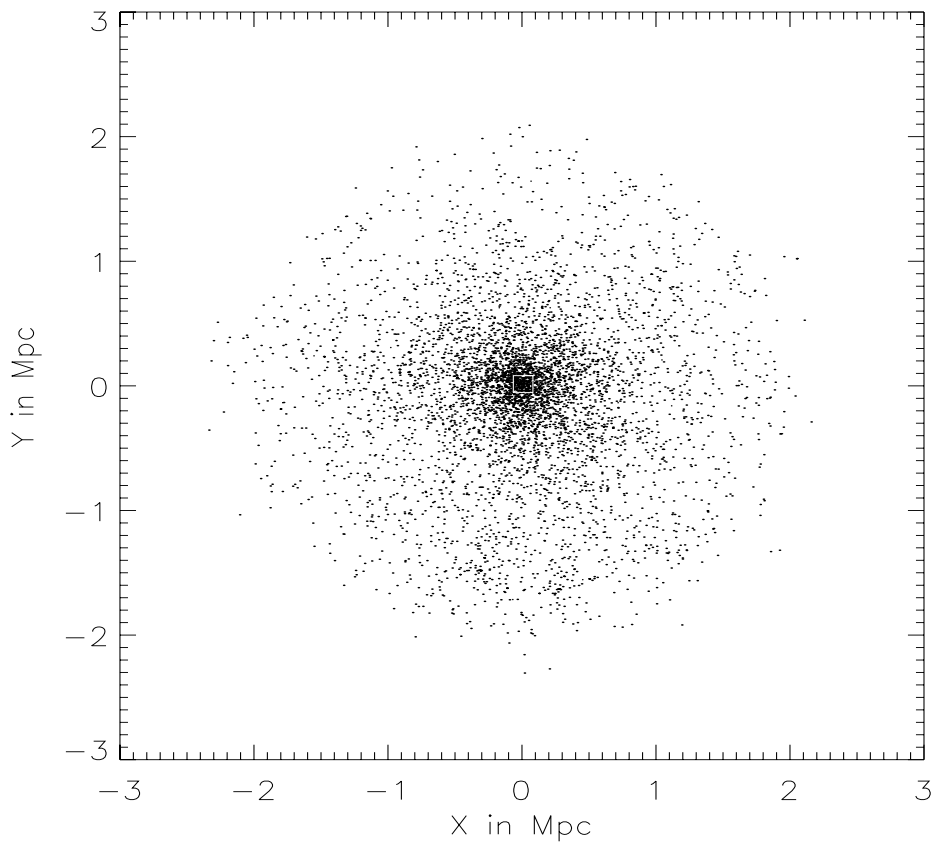

Figure 5.1: The Composite cluster made from the subsample of 45 clusters from the RASS-SDSS cluster sample, which have a central BCG

are applied to define the $R_e - \sigma$ relation used for the scaling of the of the galaxies according to velocity and radius. Only 45 out of the 78 clusters posses a central BCG. These 45 clusters are scaled and combined in the composite cluster depicted in figure 5.1. This contains a total number of 5521 galaxies. Since all the clusters participating in the composite cluster have been scaled relative to a standard cluster with $\sigma = 500$ km/s, nearly all galaxies in the standard cluster have positions inside a radius of 2 Mpc from the centre. 29 out of the 45 clusters have velocity dispersions $\sigma < 750$ km/s and the remaining 16 clusters have $750 \leq \sigma \leq 1500$ km/s.

Figure 5.2 shows a plot of type A where the mean velocity of the RASS-

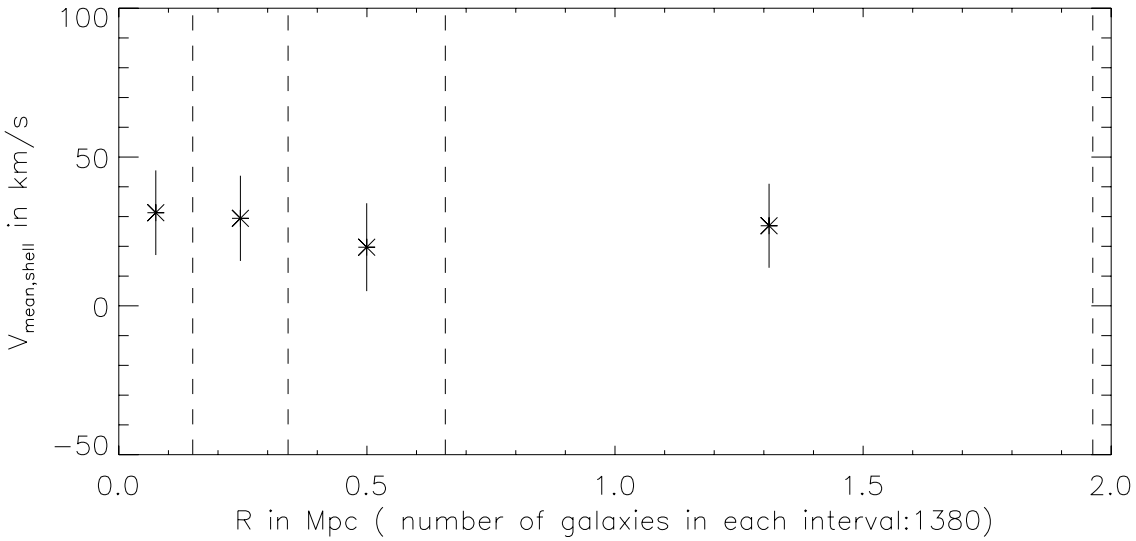

Figure 5.2: The mean velocity calculated in four shells each containing 1380 galaxies. Dashed lines indicate the outer boundary of the shells and the error bars give the standard error in each shell.

SDSS composite cluster is calculated in four shells each inclosing 1380 galaxies. The plot displays a mean velocity in all shells with a value of $20 - 30$ km/s. Within the uncertainties, this is more or less consistent with the values of $5 - 20$ km/s for the gravitational redshift predicted for a $\sigma = 500$ km/s cluster, by analytical calculations and simulation results.

Figure 5.3 shows a plot of type B. Here the mean velocity of the composite cluster is calculated stepwise as described above. The point of main interest in this plot is given by the last step, where the mean velocity of all cluster galaxies is determined. The offset of the mean in this step, relative to the zero point given by the BCGs, would be expected to be smaller than in the outer shell of the A type plot, since it will include a larger number of galaxies with positions near the centre. Still if a gravitational redshift is present, the offset should be greater than zero and the large number of galaxies included, should lower the uncertainties significantly. Figure 5.3 displays a value of about 25 km/s for the mean velocity in the last step, with an error that allow a detection well inside the 2σ-level.

With regard to the expected rise at a short distance from the centre, it

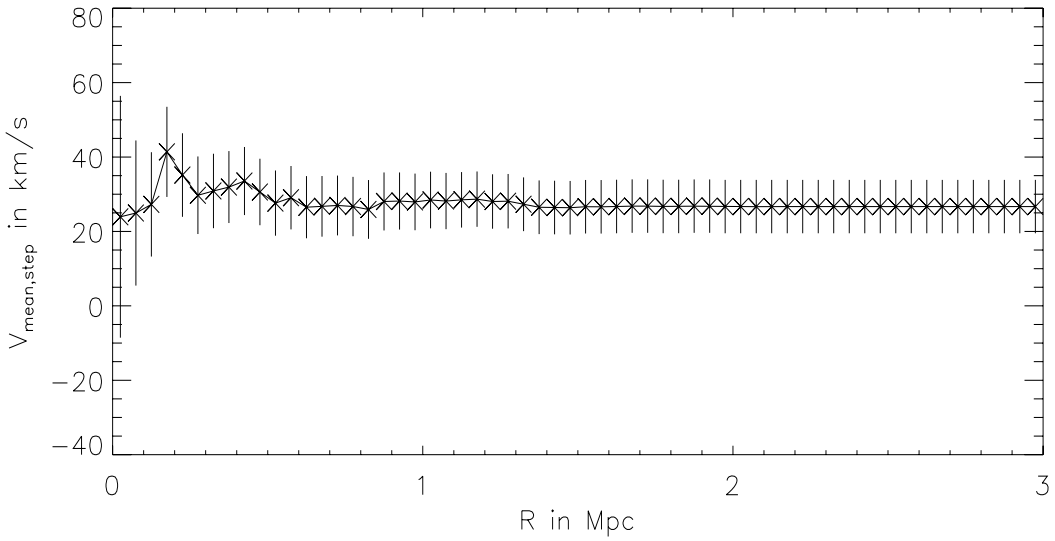

Figure 5.3: The mean velocity calculated stepwise for the RASS-SDSS composite cluster

is not possible to draw any conclusions base on Figure 5.3, because of the rather large uncertainties in the central area of the plot.

In order to compare the results of the RASS-SDSS sample with the Two subsamples of the Abell sample, I have divided the RASS-SDSS clusters having a central BCG in two subsamples consisting of the 16 clusters having $750 \leq \sigma < 1500$ km/s (RASS1) and of the 29 clusters with $\sigma < 750$ km/s (RASS2) respectively.

Two composite clusters are formed from these two subsamples. The Rass1 cluster containing 1906 galaxies and the Rass2 cluster consisting of 3619 galaxies. The mean velocities in four shells of the composite clusters are calculated and the results are plotted and displayed in figure 5.4 and 5.5. For both composite clusters the mean velocities are also calculated stepwise and plots of type B are displayed in figure 5.6 and 5.7. From the figures it is seen that the high dispersion cluster Rass1 shows a rising mean velocity out through the cluster reaching a value of about 80 km/s in the outer shell, whereas the low dispersion cluster Rass2 only has a significant mean velocity offset in the first shell near the centre. When interpreting the mean velocity offset as a result of gravitational redshift in the cluster, there is no surprise in

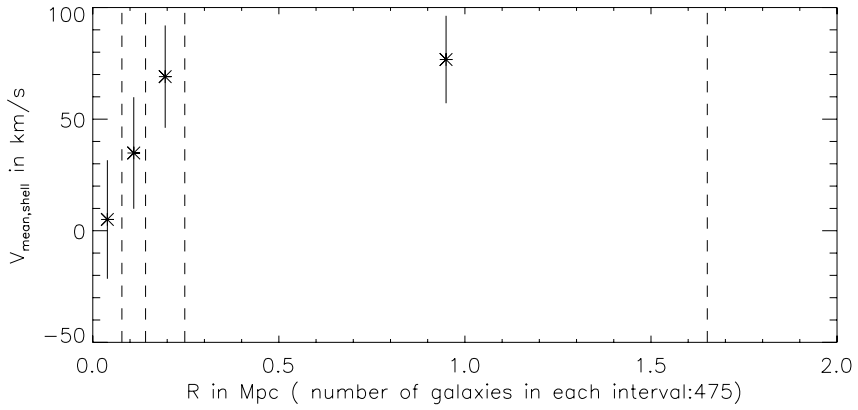

Figure 5.4: The mean velocity in four shells for the RASS1 composite cluster.

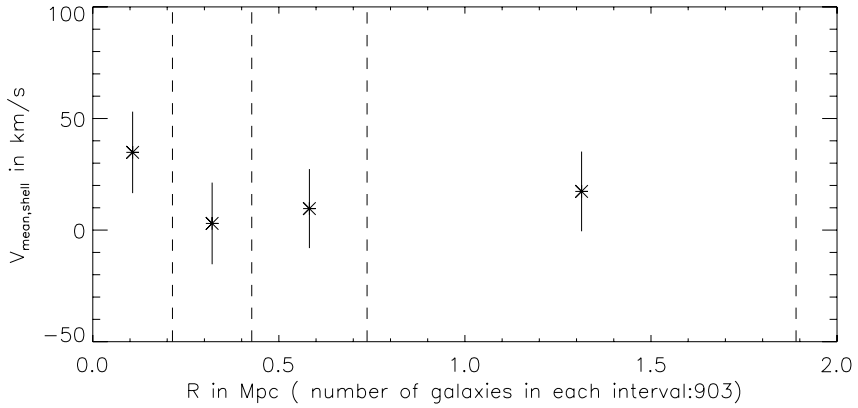

Figure 5.5: The mean velocity in four shells for the RASS1 composite cluster.

finding that the effect is greater in the high dispersion cluster. Clusters with higher velocity dispersion will in general also be the most massive and since the effect of gravitational redshift scales with mass a greater mean velocity offset should result. The value of 80 km/s for the Rass1 cluster is some what higher than what could be expected from simulations and analytical calculations, but since this composite cluster only include 16 clusters it is quite possible that high peculiar velocities in a few of the BCGs might influence the result significantly. Furthermore the sample contains two very massive

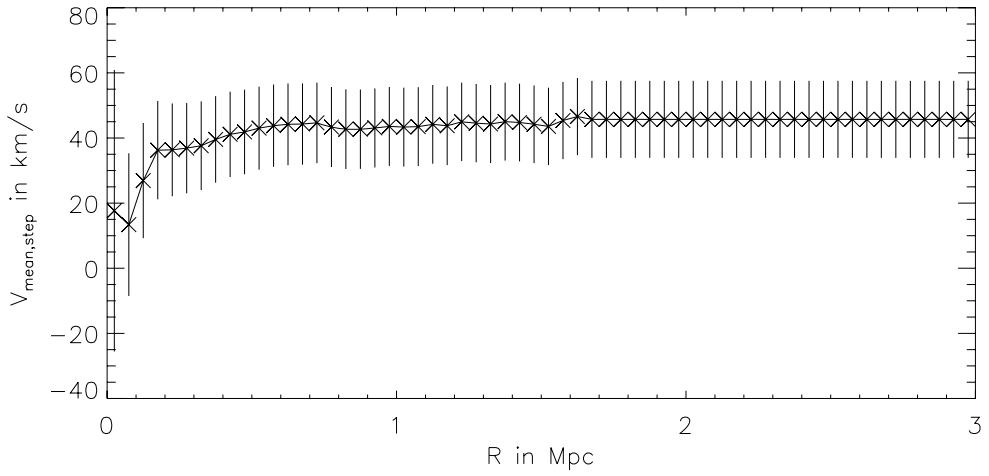

Figure 5.6: The mean velocity calculated stepwise for the RASS1 composite cluster containing 1960 galaxies

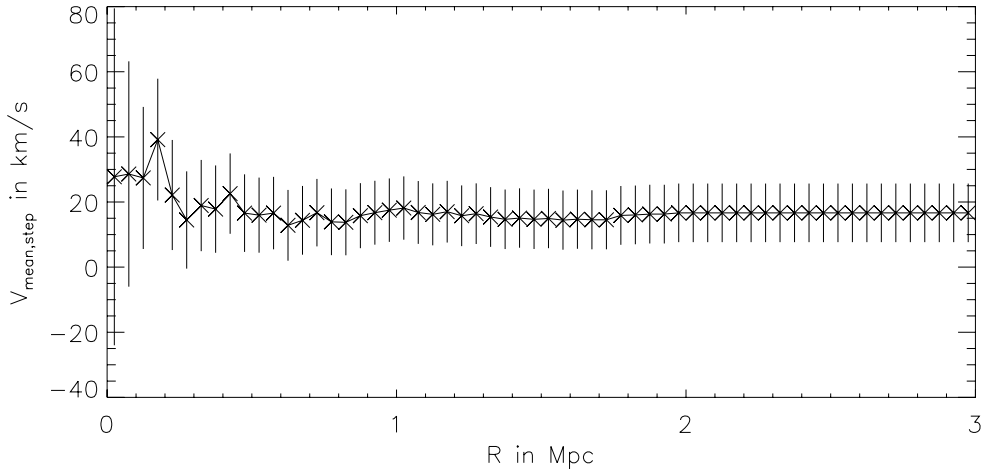

Figure 5.7: The mean velocity calculated stepwise for the RASS2 composite cluster containing 3619 galaxies

clusters with $\sigma > 1250$ and these should also tend raise the observed mean significantly.

5.2 The Abell samples

Initial near name searches are made in NED for a large number of well studied clusters with central BCGs and the result of these are passed through the Hartog and Katgert selection procedure described in the previous chapter. The result of this are the following two subsamples:

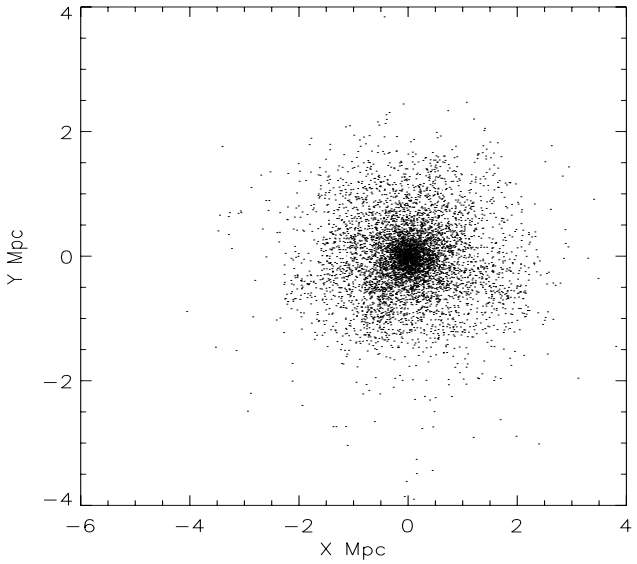

Figure 5.8: The Abell1 composite cluster containing 6139 *galaxies.*

- The Abell1 subsample consisting 31 clusters with a minimum of 60 member galaxies with redshift less than 0.1 and velocity dispersion between 750 km/s and 1250 km/s. For 68 percent of the sample the central BCGs are classified as either a cD or a D galaxy.

- The Abell2 subsample of 43 clusters with a minimum of 53 members, with redshifts less than 0.1 and velocity dispersions between 250 km/s and 750 km/s. For 49 percent of the sample the central BCGs are classified as either a cD or a D galaxy.

Four of the clusters in the Abell sample are also included in the RASS-SDSS sample.

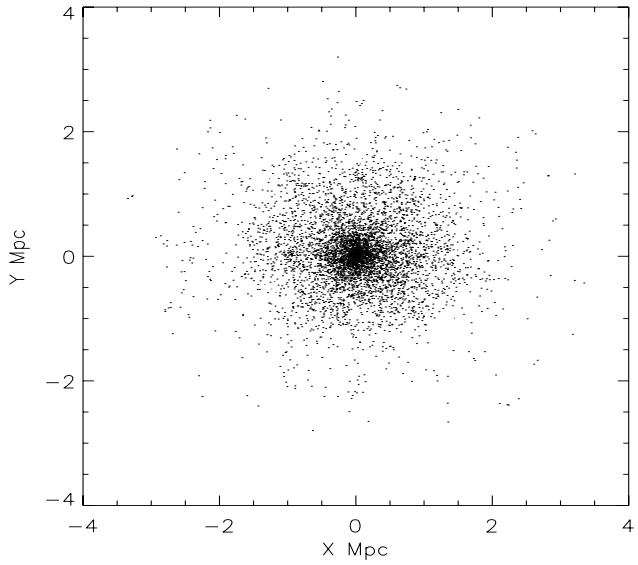

Figure 5.9: The Abell2 composite cluster containing 5655 *galaxies*

A composite cluster is constructed for each of the two subsamples. No scaling are applied in these cases, since the clusters in each subsample are assumed to be in a velocity dispersion interval that is narrow enough for the gravitational redshift in the clusters to be comparable. The two composite clusters Abell1 and Abell2 are displayed in figure 5.8 and 5.9.

The mean velocity of the two composite clusters is calculated in four shells and the result of these calculations is plotted in figure 5.10 and 5.12. The mean is also computed stepwise for both clusters and the results of this are shown in figure 5.11 and 5.13 respectively. For the high velocity dispersion cluster Abell1 no systematic rise in the mean out through the four shells is seen and the uncertainties of the mean plotted in the four shells are to large allow any detection of a significant mean velocity offset within a 2σ level relative to the zero point given by the velocities of the BCGs.

For the mean computed stepwise and displayed in figure 5.11 a value of about 20 km/s is found for the total cluster, which is very nearly within the 2σ level. This value lies within the interval of about $15-50$ km/s predicted by simulations and analytical calculations for a cluster with velocity dispersion $\sigma = 1000$ km/s.

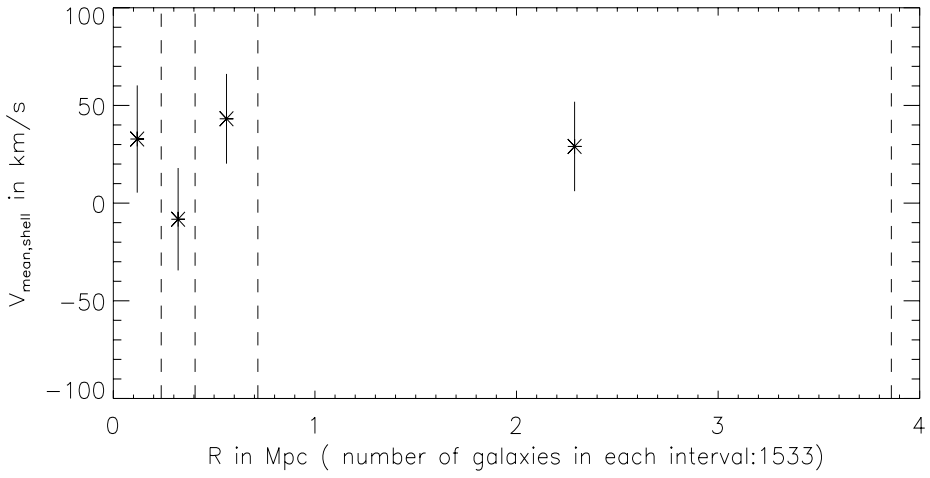

Figure 5.10: The mean velocity in four shells for the Abell1 composite cluster.

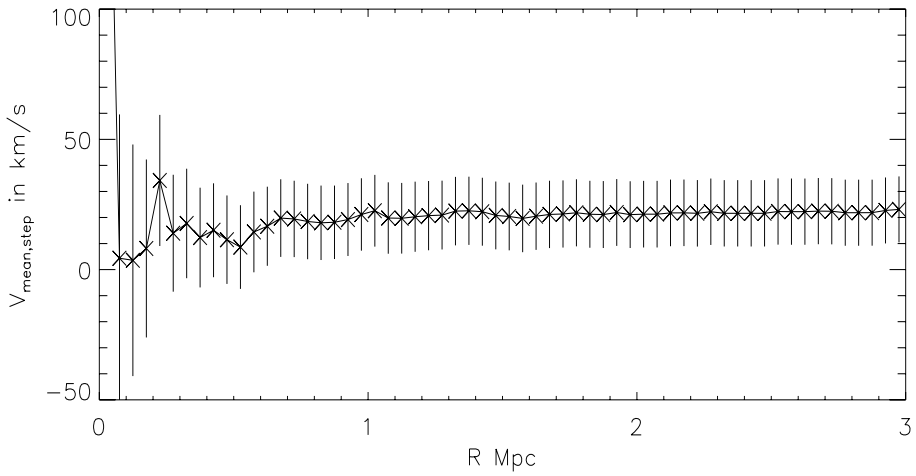

Figure 5.11: The mean velocity calculated stepwise for the Abell1 composite cluster.

For the Abell2 composite cluster a negative offset in the mean velocity are found for both calculations. The mean velocity offset calculated stepwise has a magnitude of -25 km/s when all galaxies are included. If uncertainties

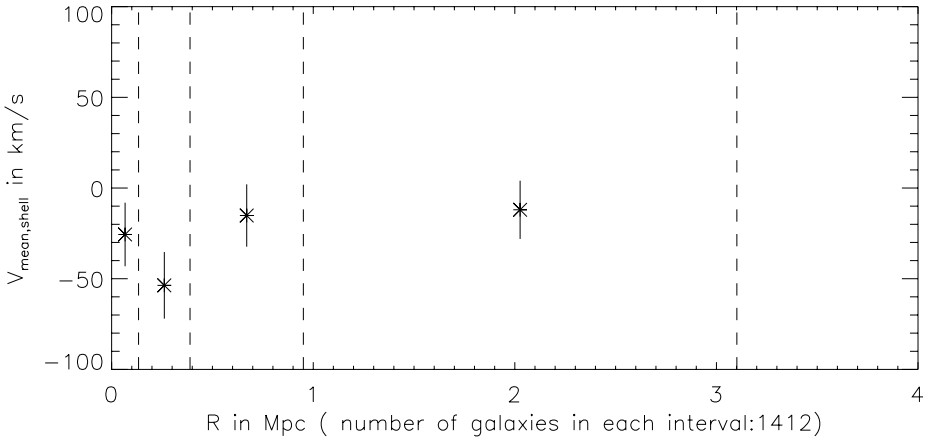

Figure 5.12: The mean velocity in four shells for the Abell2 composite cluster.

are assumed to be due only to the random movements of the galaxies, this value is well inside a 3σ level of detection. This seems to indicate that other sources of uncertainty given by peculiar velocity of the BCGs and movement of the galaxies resulting from substructure are non-neglectable and needs to be corrected for if a detection of the effect of gravitational redshift should be made for this sample.

Some of the assumed central BCGs might in reality be field galaxies or galaxies from other clusters seen in projection. It is reasonable to expect that such galaxies would primarily be in the foreground of the cluster, since their quite large brightness might result from them being closer than the rest of the cluster. If such falsely defined central BCG are foreground galaxies, they would be at a lower redshift and this would lead to the measurement of a negative velocity offset relative to the cluster mean. This would then lower the total offset for a composite cluster having the false central BCGs as participants.

cD and D galaxies are believed to exist only in the centre of clusters so when considering composite clusters consisting of only clusters having cD or D galaxies as their central BCG, the above pollution from foreground BCGs might be avoided and an increase in velocity offset for the composite cluster might be expected. To test this, two subsamples containing only cD and D galaxies as BCGs were constructed. The first sample Abell11 consist of all 21 cluster from The Abell1 sample having cD or D galaxies as their central

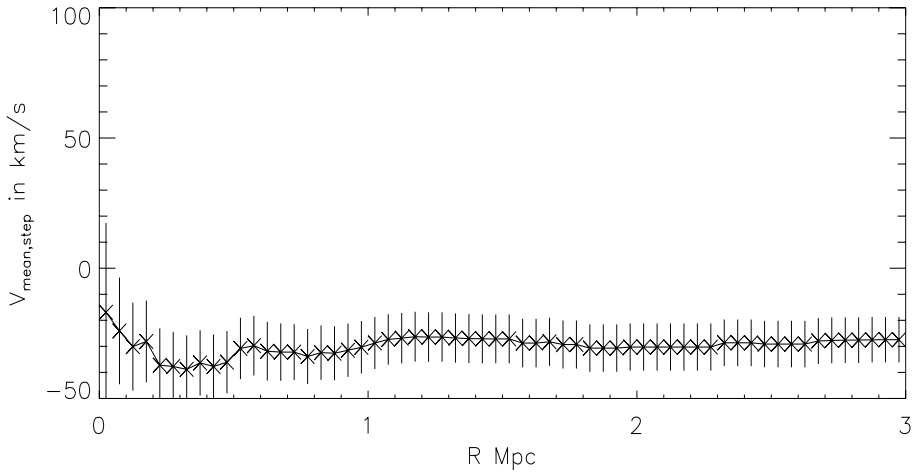

Figure 5.13: The mean velocity calculated stepwise for the Abell2 composite cluster.

BCG and the second sample Abell22 is made of 22 cD or D clusters from the Abell2 cluster sample.

The mean velocity offset is computed stepwise for the composite clusters constructed from the Abell11 and Abel22 samples. The results of this are displayed in figure 5.14 and 5.15. The offset in the mean velocity relative to the BCGs is seen to increase in both composite clusters compared to what were found for the Abell1 and Abell2 composite clusters. If the increases can be interpreted as resulting solely from the removal of false defined central BCGs, the effect of the pollution from these is clearly non-neglegtable and should be taken into account. Still putting to much faith in this interpretation might be to optimistic, considering the limited size of the two cD/D cluster subsamples.

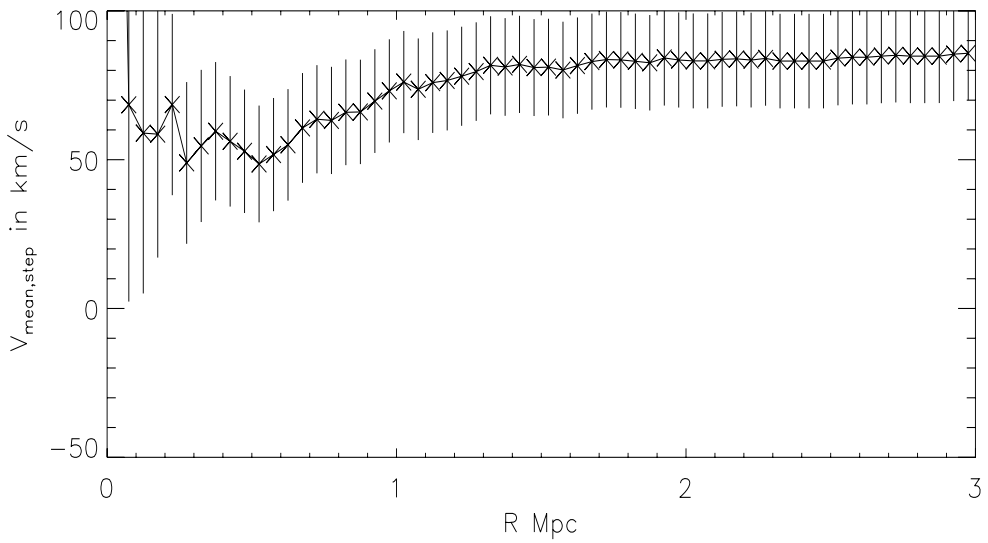

Figure 5.14: The mean velocity calculated stepwise for the Abell11 composite cluster consisting 21 cD and D galaxies.

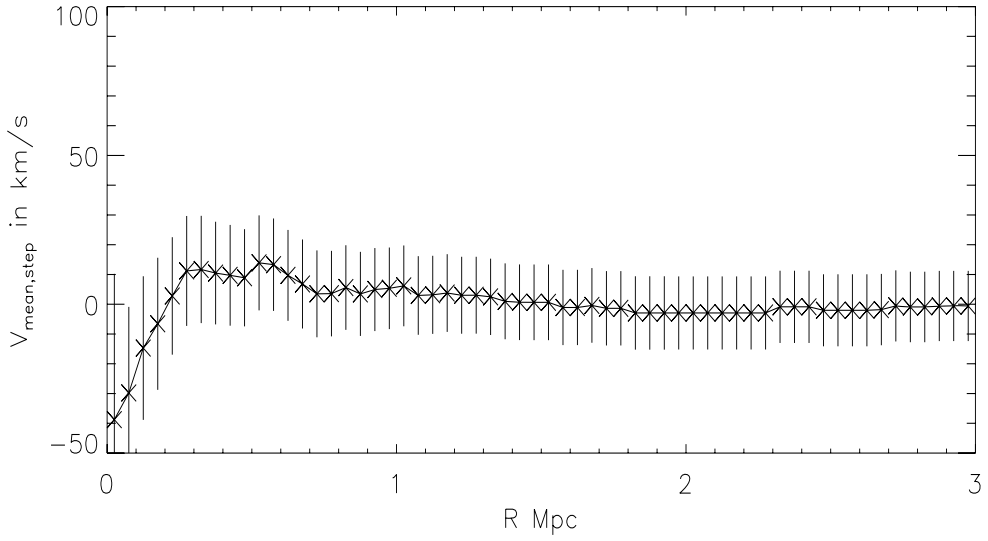

Figure 5.15: The mean velocity calculated stepwise for the Abell2 composite cluster consisting 22 cD and D galaxies.

Chapter 6

The Movement of the cD

In order to examine whether the idea of a central galaxy nearly at rest in the centre of the cluster is an overall reasonable assumption, I will try to find an estimate of the typical magnitude of the peculiar velocities of the central galaxies. I will look at the following aspects:

- For central galaxies classified as cD-galaxies there are several theories concerning their formation. I will make a short review of these, in order to asses the possible influences on the current peculiar velocities.
- A number of authors have studied the peculiar velocities cD galaxies and I will make a brief summary of their results.
- In cases where the galaxy is not a cD, a scenario where the galaxy is formed elsewhere and then brought to the cluster centre after formation might be a possibility. In order to investigated whether this could lead to a central galaxy at rest in the potential minimum, I've made a short iterative calculation based on this scenario.
- Last but not least I consider the peculiar velocities of the central galaxies in the samples used in the last chapter.

6.1 Formation of cD-galaxies

In regard to the formation of cD-galaxies four different formation scenarios have been proposed (Sarazin [28] and Garijo et Al [10]):

1. In clusters with a sufficiently high central density the intracluster gas from cooling flows, can gradually condense and form stars at the centre of the cluster. If a galaxy is present at the centre, the stars will be accreted on to it and thereby form a bright, extended object.

   The ongoing star formation should be visible as a colour gradient out through the galaxy and such gradients has been observed in some cD-clusters.

2. Another possible formation scenario suggests that the cD galaxies arise as a result of mergers between clusters, in which some of the cluster galaxies are captured by larger central galaxies originally residing in one or both of the merging clusters. Dynamical friction in combination with the merger, could be expected to create a central merger product, that would be at rest in the centre of the potential of the merged clusters. Kinetic energy released in the merger, would heat up the central object and inflated it and thereby increase its radius. This would create a large central galaxy with a high luminosity, which would resemble the central object in a cD.

   If the merger scenario is correct it would be reasonable to expect that a significant number of cDs would show evidence of mergers in the form of multiple nuclei. This turns out to be in accordance with observation, which finds multiple nuclei in more than 1/4 of all cD clusters [28]. The merger scenario however does not account for the extended halo observed around the central galaxy in the cDs.

3. When the galaxies in a cluster passes close to the centre of the potential tidal effects might cause matter in the form of dark matter, stars and gas in the outer envelope of the galaxies to be torn off. If a galaxy is residing at the centre of the potential, this galaxy might accrete the tidally striped material. This might form an extended halo around the galaxy, similar to what is observed in cD-galaxies. Since the stripped material would originate from galaxies passing by from all directions, it could be expected to be evenly distributed around the potential minimum and should therefore be more or less at rest relative to this.

   There are two problems facing this scenario. First it only explains the existence of the halo of the cD and does not account for the size and brightness of the central galaxy. Secondly the velocity dispersion of the

stars in the cD, are significantly lower than in the other galaxies, a fact that the scenario does not account for.

4. A fourth alternative points out, that after the cluster collapse a high fraction of the mass in the cluster background and relatively high velocities between cluster galaxies, would tend to limit the merging processes. This would in turn inhibit the growth of a centrally dominant galaxy. The suggestion in this scenario is therefore that the formation process must have taken place before the cluster collapsed.

Nearly all these scenario assumes the existence of a proto cD, initially positioned in the centre of the potential.

Garijo et al [10] studies N-body simulations of groups of galaxies in order to investigate how different initial conditions and different types of collapse scenarios affect the formation of a centrally located massive galaxy. They find that if the initial conditions include a central seed, then a massive central galaxy is created every time.

If cD-galaxies are "born" in the centre of the potential of an emerging cluster, it would be fair to assume that they generally have low peculiar velocities relative to the minimum of the cluster potential. If this were the case it would render them highly useful as indicators of the central gravitational redshift in their host clusters.

6.2 Studies of cD peculiar velocities

Bird [5] studies a sample of 25 cD clusters with a minimum of 50 redshifts per cluster. She finds that 32 percent of the cDs have significant peculiar velocities relative to the mean velocity of the cluster galaxies. She proposes that this is due to the mass dependence of dynamical friction. As a result of the fairly high mass of the growing central object/cD, the process of dynamical friction will act on it on a relatively short timescale, when mergers between clusters occur. The rest of the galaxies belonging to the two clusters will retain evidence of their original distribution in distinct subclusters for a longer time, because of their considerably smaller masses. This may lead to an error in the estimation of The cDs velocity relative to the cluster mean, since velocity contributions resulting from the subclustering might add to the random velocities of the cluster galaxies.

Bird uses a partitioning algorithm to assign the cluster galaxies to their "host" subclumps and she then determines their velocities as the velocity relative to their "host". She finds that with this correction for substructure, only two out of the 25 clusters considered have a cD with a significant peculiar velocity, relative to the cluster mean.

Oegerle and Hill [21] make a corresponding survey of another sample of 25 cD clusters with a minimum of 43 redshifts. 13 of these cluster are also included in the sample used by Bird. Oegerle and Hill find that after corrections for substructure have been made, only 4 clusters have cDs with significant peculiar velocities.

The results of both Bird and Oegerle and Hill seems to indicate that most cD galaxies are actually more or less at rest relative to the centre of the potential. Still it seems premature to make any decisive conclusions based on these results, since both of the two studies were only based on a rather limited number of clusters.

6.3 The movement of non-cD BCGs

As was described above, the proposed formation scenarios for cD galaxies seems to indicate that the cDs are "born" in the centre of the cluster potential. A significant number of the BCGs used in the cluster samples of this thesis are however not classified as cDs and it therefore seems sensible to consider the peculiar velocities of central BCGs, which have not been formed in the centre of the cluster, but have arrived there at a later time. In order to do this, I have made a simple calculation, to get a sense of the timescale on which dynamical friction decrease the speed of an infalling massive galaxy and drags it to the centre.

A NFW distribution is assumed for the cluster and the BCG is initially placed at a distance of $2-3$ Mpc from the centre, depending on the mass of the cluster. The resulting forces from the gravitational potential and from dynamical friction are calculated and from this the change in position and velocity of the BCG is determined. This is done repeatedly, by stepping the calculation forward in time, using a leap-frog algorithm. The procedure is performed for a time interval of 10 Gyr, with a time step $\Delta t = 10^{-6}$Gyr. In figure 6.1 and 6.2 the result of these calculations are shown for two clusters. The first (figure 6.1)has a mass of $M = 1\times10^{15}\mathrm{M}_{\odot}$, a, BCG mass of $M_{BCG} = 1\times10^{12}\mathrm{M}_{\odot}$, a concentration parameter $c = 5.0$ and a BCG is placed initially

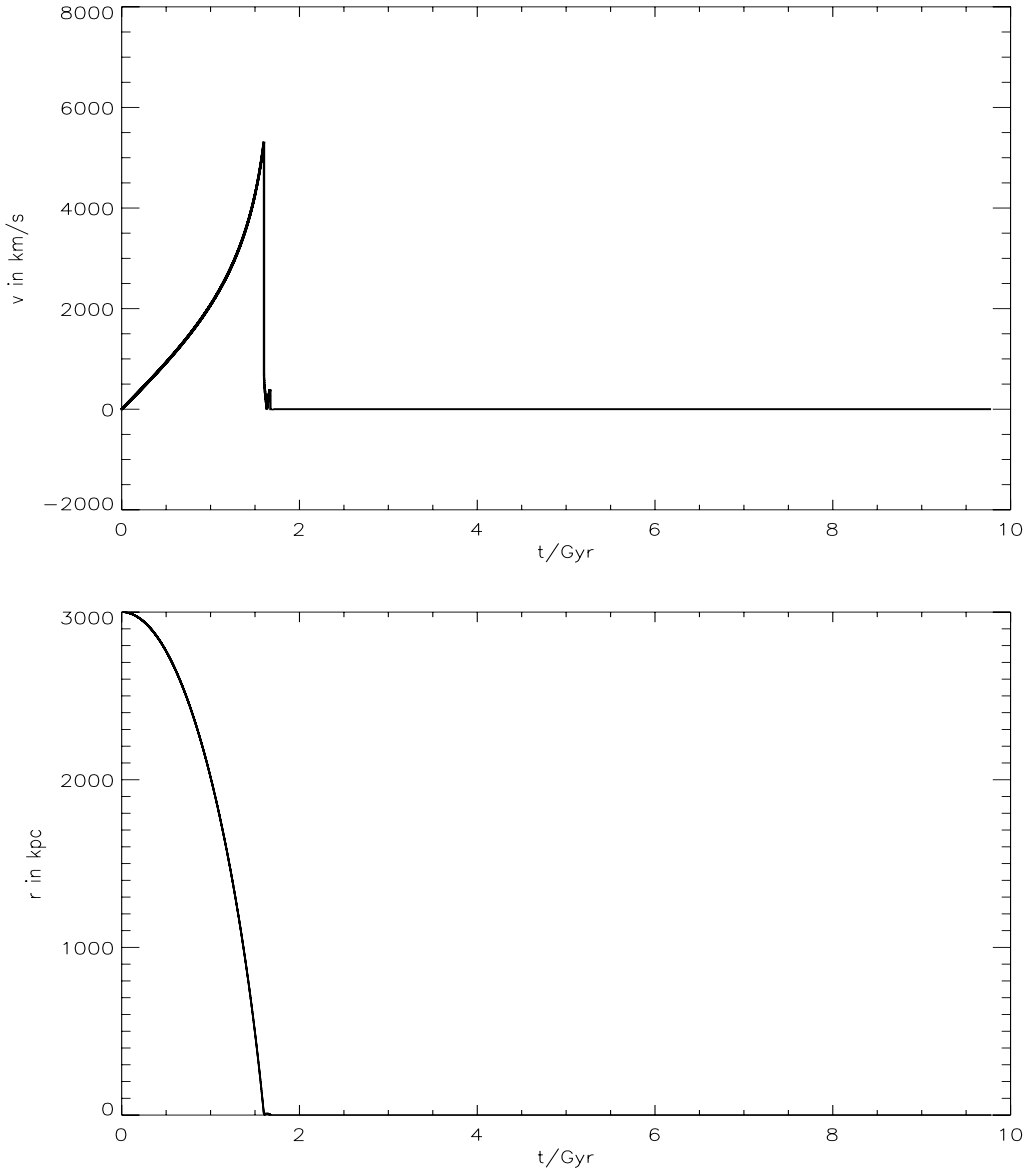

Figure 6.1: The velocity and position of an in falling massive galaxy with $M = 1. \times 10^{12} \mathrm{M}_{\odot}$ *influenced by dynamical friction in a NFW-potential, with* $M_{200} = 1. \times 10^{15} \mathrm{M}_{\odot}$ *and concentration parameter c= 5, as a function of time.*

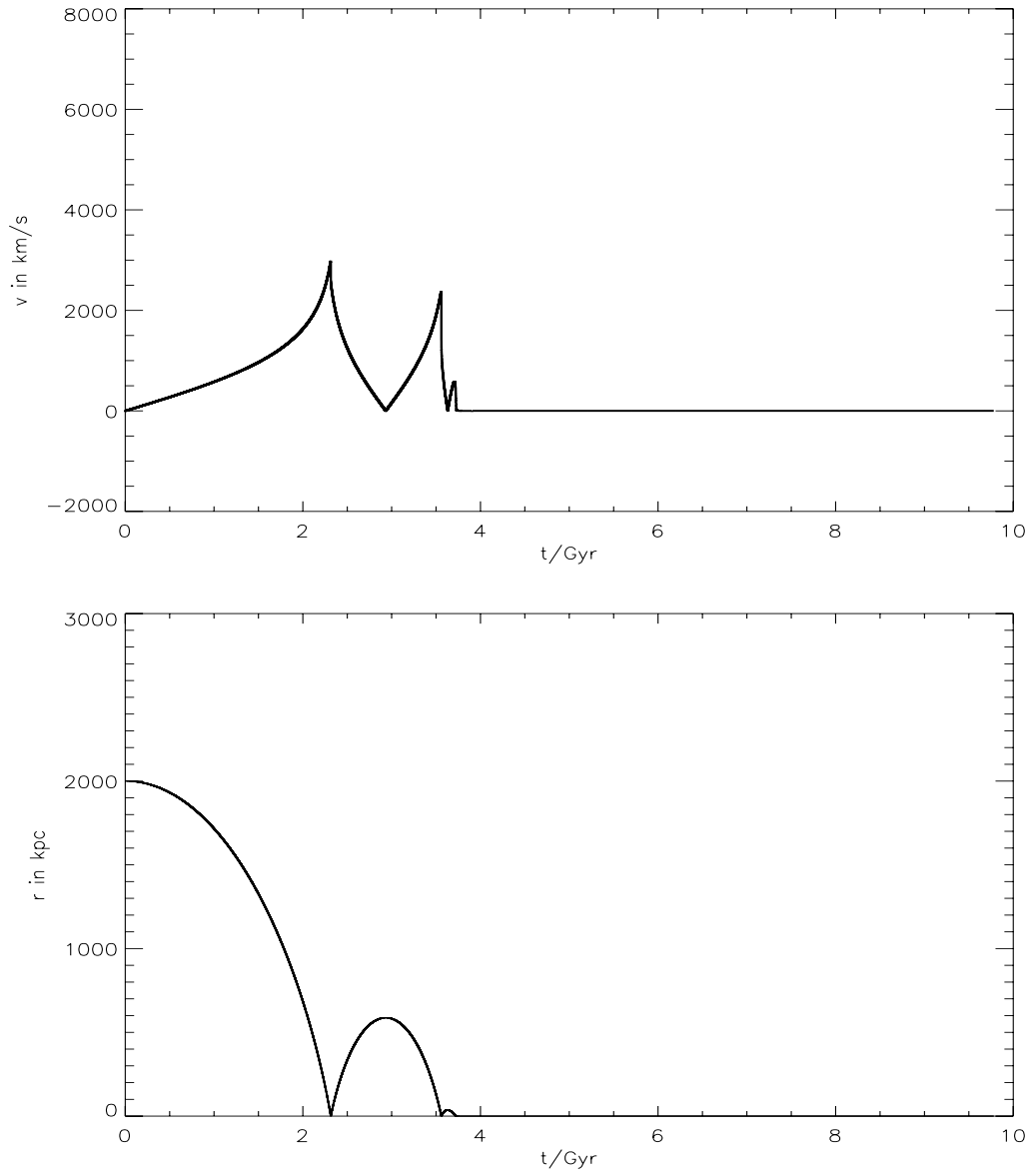

Figure 6.2: The velocity and position of an in falling massive galaxy with $M = 1. \times 10^{11} \mathrm{M}_{\odot}$ *influenced by dynamical friction in a NFW-potential, with* $M_{200} = 1. \times 10^{14} \mathrm{M}_{\odot}$ *and concentration parameter c= 8, as a function of time.*

at rest at a radius of 3 Mpc. For the second cluster shown in figure 6.2 the mass is $M = 1 \times 10^{14} \mathrm{M}_{\odot}$, the BCG mass is $M_{BCG} = 5 \times 10^{11} \mathrm{M}_{\odot}$, the concentration parameter has the value $c = 8.0$ and the BCG is started at a radius of 2 Mpc. The figures show that the massive cluster is slowed down on a relatively short timescale, while the less massive cluster takes somewhat longer to come to a halt in the centre of the potential. This might indicate that the BCGs in less massive clusters would maintain a significant peculiar velocity, for a longer period of time. This is in accordance with dependence of dynamical fiction on both the mass density of the cluster and the mass of the BCG. This might to some extend explain why the effect of gravitational redshift can not be detected in many low velocity dispersion clusters as was observed in the last chapter. Yet one must of course bear in mind that the above, is result of a highly simplified calculation, where for instance the effect of mass loss of the BCG as a result of interaction with other galaxies or with the cluster background, has not been taken into account.

6.4 Peculiar velocities of the three applied samples

To get a sense of the typical magnitude of the peculiar velocities of central BCG galaxies I have made velocity histograms for each of the three cluster samples used in the previous chapter. This are displayed in figure 6.3, 6.4 and 6.5. In all three figures close to 80 percent of the BCGs have absolute velocities in the range $0-250$ km/s. The RASS-SDSS cluster sample and the Abell2 cluster sample are more centrally peaked with 70 percent of the BCGs having absolute velocities in the range $0-150$ km/s compared to the Abell1 sample where only about 50 percent of the BCGs have absolute velocities in this range.

The dispersions for the velocities in the three samples are between 173 km/s to 225 km/s. Since the velocities of the BCGs are taken relative to the cluster mean, it is not possible to separated contributions to the dispersion resulting from actual movements of the BCGs relative to the cluster centre, from contributions due to uncertainties in the determination of the mean velocity of the cluster and from systematic substructure movements of the cluster galaxies. Still the rather large number of BCGs having non-neglectable velocities could indicate that the uncertainties resulting from the

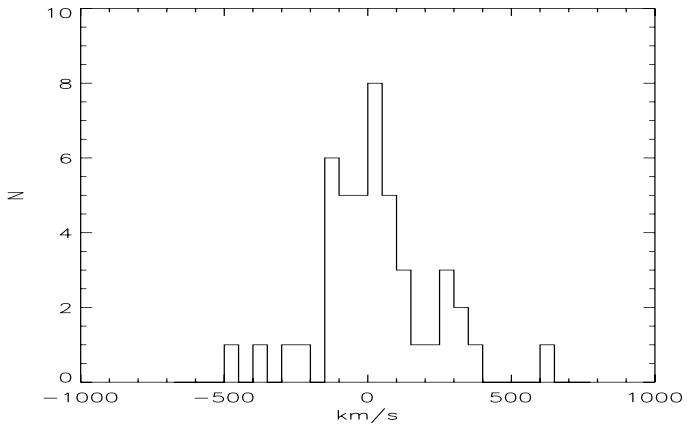

Figure 6.3: The BCG velocity relative to the cluster mean velocity for the clusters in the RASS-SDSS sample

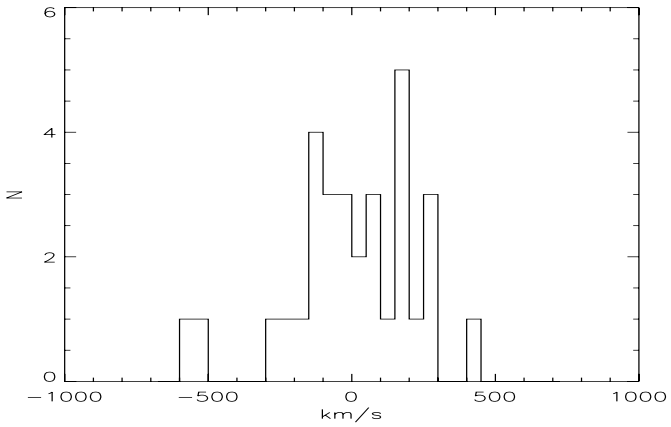

Figure 6.4: The BCG velocity relative to the cluster mean velocity for the clusters in the Abell1 sample

peculiar movement of the BCGs will be of importance for cluster samples of the sizes considered in this thesis and that a larger cluster sample might be needed in order to make a certain detection of a velocity offset resulting from gravitational redshift.

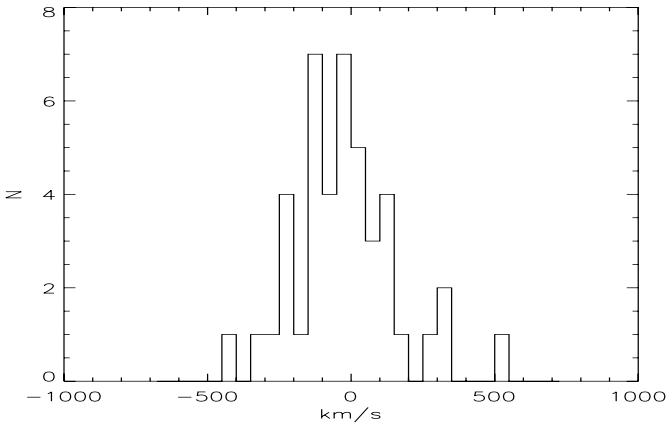

Figure 6.5: The BCG velocity relative to the cluster mean velocity for the clusters in the Abell1 sample

Chapter 7

Summary and discussion

7.1 Summary

In this thesis I have been considering the possibility of measuring the effect of gravitational redshift in clusters of galaxies. I have been doing this by finding predictions for the effect in simulated clusters and from analytical calculations based on two different density distributions. This points to a gravitational redshift velocity in the range $5 - 50$ km/s. I have compared these predictions with results from composite clusters created from three different data samples, consisting of clusters having a centrally located BCG galaxy.

For a composite cluster consisting of massive clusters with velocity dispersion above 750 km/s, a significant positive velocity difference between the BCGs and the cluster mean in the range $25 - 80$ km/s is found, whereas the case for less massive clusters is more ambiguous and displays both positive and negative values for the velocity difference between BCGs and cluster mean.

For the individual clusters the velocities of the central galaxies relative to the mean velocity in their respective clusters are found to lie in the approximate range $0 - 650$ km/s, with 80 percent in the velocity range $0 - 250$ km/s. This is in agreement with what is found for the two simulated cluster, where the cD velocities relative to the cluster mean are 186 km/s and 248 km/s for the two clusters respectively.

7.2 Discussion

When considering the results of my attempts to detect the effect of gravitational redshift in three samples of galaxy cluster, the following points seems worth mentioning:

- Within the uncertainties given by random movement of the cluster galaxies, the mean velocity offset relative to the velocity of the central galaxy in massive clusters have a positive value within a 2σ level and is reasonably consistent with the predicted magnitude of the gravitational redshift velocity found in the simulations and from the analytical calculations.

- In less massive cluster with mass less than $M \simeq 10^{14}\mathrm{M}_{\odot}$ it seems more difficult to detect an effect. This might be due to the lower magnitude of the effect of gravitational redshift in these clusters, but it could also be a result of the mass dependence of the time scales of dynamical friction. The latter might lead to a higher degree of systematic movement in the cluster, which would add to the noise when trying to detect the gravitational redshift. All in all the negative offset seen for the less massive clusters point to the existence of uncertainties, which have not been taken into account. Overall considerations of formation scenarios for cD galaxies suggests that these could be expected to be nearly at rest relative to the cluster centre. Yet both the result of the simulations and the evaluation of the BCG velocity relative to the mean in the individual clusters seems clearly to indicate that these velocities, whether due to actual movement of the BCG or systematic movements of the other cluster galaxies, must somehow be corrected for if a certain detection of the gravitational redshift should be obtained.

- Considering the scaling procedure used for the scaling of the RASS-SDSS cluster sample, it is not clear whether this could have some influence on the offset between the mean velocities of clusters and the BCG velocities. The relation between R_e and σ is very poorly defined for $\sigma > 900$ km/s and when the RASS-SDSS BCG cluster sample was split into high and low σ subsamples a quite large difference in velocity offsets was found between the two subsamples, compared to the difference found for the two Abell subsamples. This might be taken to

indicate that the scaling used has some bias in favour of the more massive clusters. On the other hand the relatively small number of clusters in especially the subsample of massive clusters, make it probable that the high value of the velocity offset of the mean cluster velocity in the composite cluster relative to the BCG velocities, might be due to the influence of high peculiar BCG velocities in a few of the clusters.

- With regard to the possibility of fitting a density profile based on a potential deduced from the gravitational redshift profile, it is clear that a significantly larger number of clusters is needed in order to do this. The particular interest of such a profile would concern its development in the central part of the composite cluster. The movement of the galaxies in this area might be severely influenced by central substructure resulting from recent mergers. In addition to a higher noise level, the mean velocity has to be computed in very narrow radius intervals in order to get a detailed profile for the gravitational redshift. Since the number of redshifts that can be obtained inside a given area are limited by spectroscopic observing techniques a detailed central profile might depend strongly on having a rather large number of clusters participating in the composite cluster. From the results produced in this thesis it is evident that the size of cluster samples used here does not permit any conclusions to be drawn about the detailed central behaviour of the mean velocity offset relative to the central galaxy.

  The massive simulation cluster C2 shows a rise of about 16 km/s in gravitational redshift velocity inside the inner 0.1 Mpc. In order to detect this with a 2σ certainty, only taking uncertainties due to random movement into account and assuming as much as 20 available redshifts inside a radius of 0.1 Mpc for each cluster, it would take 800 clusters to get a standard error of the mean as low as 8 km/s.

  Since a decrease in velocity dispersion with radius is not uncommon, clusters with a total velocity dispersion around 1000 km/s might have an even higher velocity dispersion in centre and the above number of 800 clusters might therefore only be a lower limit.

  If the estimate of the number of available massive clusters made by Kim and Croft [17] is correct, there are only about 600 such clusters in the observable universe and if so it would clearly be impossible to get a detailed profile with a reasonable certainty.

Creating a detailed profile for the less massive clusters might be feasible. The less massive simulation cluster C1 displays a rise of about 8 km/s, so a 2σ detection would take about 1500 clusters with velocity dispersion $\sigma \simeq 500$, if a minimum of 10 galaxies inside the inner 0.1 Mpc is assumed. Since there are a far greater number of low mass compared to high mass clusters, 1500 low mass cluster might not be impossible to obtain

All in all the above problems show that there several sources of difficulty in attempting a detection of gravitational redshift in galaxy clusters and that it might be questionable whether the assumption of random movements as the sole source of uncertainties is reasonable.

If further work on the subject of gravitational redshift in galaxy clusters should be attempted, one possibility would be to focus on reducing the uncertainties due to systematic movements of the cluster galaxies. This might either be done by making corrections for substructure as was done by Bird [5], or by assembling a set of regular massive clusters, which might have a lesser degree of the substructure.

Appendix

Chapter 8

Appendix A: The NFW-distribution

This distribution has been described and named by Navarro, Frenk and White and has the following form

$$\rho(r) = \frac{\rho_{crit}\delta_c}{\frac{r}{r_s}(1+\frac{r}{r_s})^2} \tag{8.1}$$

and by integration the potential can be expressed as

$$\begin{aligned}
\phi(r) &= -4\pi G\left(\frac{1}{r}\int_0^r \rho(r)r^2dr + \int_r^{R_t}\rho(r)rdr\right) && (8.2)\\
&= -4\pi G\left(\frac{1}{r}\int_0^r \frac{\rho_{crit}\delta_c}{\frac{r}{r_s}(1+\frac{r}{r_s})^2}r^2dr + \int_r^{R_t}\frac{\rho_{crit}\delta_c}{\frac{r}{r_s}(1+\frac{r}{r_s})^2}rdr\right) && (8.3)\\
&= -4G\pi\rho_{crit}\delta_c\left(\frac{r_s^3(r+(r+r_s))}{r(r+r_s)} * \ln\left(\frac{r_s}{r_s+r}\right)\frac{r_s^3(r-R_t)}{(r+r_s)(r_s+R_t)}\right)\\
&= -\frac{4\pi G\rho_{crit}\delta_c r_s^3}{r(r_s+R_t)}\left(r+(r_s+R_t)\ln\left(\frac{r_s}{r+r_s}\right)\right) && (8.4)\\
&= -\frac{4\pi G\rho_{crit}\delta_c r_s^3}{(r_s+R_t)}\left(1+\frac{(r_s+R_t)\ln\left(\frac{r_s}{r+r_s}\right)}{r}\right) && (8.5)
\end{aligned}$$

When $r \to 0$, the potential approach constant value, which can be shown as follows

First consider the expression

$$Lim_{r\to 0}\left(\frac{\ln\left(\frac{r_s}{r_s+r}\right)}{r}\right) \tag{8.6}$$

Since we are looking at small values of r, we most have that$\frac{r_s}{r_s+r} \sim 1$ Therefore one can make an expansion of $\ln\left(\frac{r_s}{r_s+r}\right)$, whit the aid of the expression

$$\ln(x) = \left(\frac{x-1}{x}\right)+\frac{1}{2}\left(\frac{x-1}{x}\right)^2+\frac{1}{3}\left(\frac{x-1}{x}\right)^3\cdots\cdots, x\geq\frac{1}{2} \tag{8.7}$$

Since $\frac{\frac{r_s}{r_s+r}-1}{\frac{r_s}{r_s+r}} = -\frac{r}{r_s}$ we get that

$$\ln\left(\frac{r_s}{r_s+r}\right) = -\left(\frac{r}{r_s}\right)+\frac{1}{2}\left(\frac{r}{r_s}\right)^2-\frac{1}{3}\left(\frac{r}{r_s}\right)^3\cdots \tag{8.8}$$

and therefore that

$$\frac{\ln\left(\frac{r_s}{r_s+r}\right)}{r} = -\frac{1}{r_s}+\frac{1}{2}\frac{r}{r_s^2}-\frac{1}{3}\frac{r^2}{r_s^3}\cdots \tag{8.9}$$

$$\to -\frac{1}{r_s}, \text{ for } r\to 0 \tag{8.10}$$

and that the central value of the potential is given as

$$\begin{aligned} Lim_{r\to 0}\phi(r) &= -Lim_{r\to 0}\left(\frac{4\pi G(\rho_{crit}\delta_c)r_s^3}{(r_s+R_t)}\left(1+\frac{(r_s+R_t)\ln\left(\frac{r_s}{r+r_s}\right)}{r}\right)\right) \\ &= \frac{4\pi G(\rho_{crit}\delta_c)r_s^2R_t}{(r_s+R_t)} \end{aligned} \tag{8.11}$$

Bibliography

[1] Bahcall, D. and Tremaine, S. 1981
Methods for determining the mass of spherical systems.
ApJ., 244, 805.

[2] Bahcall, N. and Bode, P. 2003
The amplitude of mass fluctuations.
ApJ, 588, l1

[3] Beers, T.C., Flynn, K. and Gebhardt, K. 1999
Measures of location and scale for velocities in clusters of galaxies - A robust approach.
AJ, 100, 32.

[4] Binney, J. and Tremaine, S. 1994
Galactic dynamics.
Princton University Press.

[5] Bird, C.M. 1994
Substructure in clusters and central galaxy peculiar velocities
AJ, 1994, 107, 1637

[6] Broadhurst, T. & Scannapieco, E. 1999
Detecting the gravitational redshift of cluster gas.
. Astro-ph/9912412

[7] Bullock, J.S. Kolatt, T.S. Sigad, Y. et al.
Profiles of dark haloes: evolution, scatter and environment
astro-ph/9908159.

[8] Cappi, A. 1995
Gravitational redshift in galaxy clusters.
A&A, 301, 6.

[9] Coggins, S. 2003
Gravitational redshift and mass distributions of galaxies and clusters.
Doctoral thesis.
University of Nottingham.

[10] Garijo, A., Athanassoula, E. and Garcia-Gomez, C. 1997
The formation of cD galaxies
astro-ph/9705216

[11] Girardi, M., Giurcin, G., Mardirossian, F., et al. 1998
Optical mass estimates of galaxy clusters
ApJ, 505, 74.

[12] Hartog, R. D. and Katgert, P. 1996
On the dynamics of the cores of galaxy clusters.
MNRAS, 279, 349

[13] Hernquist, L. 1990
An analytical model for spherical galaxies and bulges
ApJ, 356, 359h.

[14] Katgert, P., Biviano, A. and Mazure, A. 2004
The ESO NEARBY ABELL CLUSTER SURVEY. XII
The mass and mass-to-light ratio profiles of rich clusters.
ApJ, 600, 657.

[15] Katz, N. and Hernquist, L. 1996
Cosmological simulations with TreeSPH.
ApJS, 105, 19.

[16] Katz, N., Winnberg, A. and Hernquist, L. 1989
TREESPH: A unification of SPH with the hierarchial tree method.
ApJS, 70, 419.

[17] Kim, Y. and Croft, R. 2004
Gravitational redshift in simulated galaxy clusters.
ApJ, 607, 164.

[18] Navarro, J. F., Frenk, C.S., White, S.D.M. 1997
A universal density profile from hierarchical clustering.
ApJ, 490, 493.

[19] Nottale, L. 1976
Redshift anomaly in associations of clusters of galaxies.
ApJ, 208, L103.

[20] Nottale, L. 1983
Pertubation of the magnitude-redshift relation in an inhomogeneous relativistic model.
A&A, 118, 85.

[21] Oegerle, W.R. and Hill, J. M. 2001
Dynamics of cD clusters of galaxies IV
AJ, 122, 2858

[22] Padmanabhan, T. 1993
Structure formation in the universe.
Cambridge University Press.

[23] Popesso, P., Böhringer, H., Brinkmann, J. et al. 2004
ROSAT-SDSS Galaxy Cluster Survey.
I.The catalog and the correlation of X-ray and optical properties.
A&A, 423, 449

[24] Popesso, P., Biviano, A., Böhringer, H., et al. 2005
ROSAT-SDSS Galaxy Cluster Survey.
III. Scaling relations of galaxy clusters.
A&A, 433, 432

[25] Postman, M. 1995
Brightest cluster galaxies as standard candles..
ApJ, 440, 28.

[26] Romeo, A., Portinari, L. and Sommer-Larsen, J. 2005
Simulating Galaxy Clusters -II: Global star formation and the Galaxy Populations.
MNRAS, 361, 983

[27] Rood, H.J. and Struble, M.F. 1982
Test for a richness-dependent component in the systematic redshift of galaxy clusters.
ApJ, 252, L7.

[28] Sarazin,C.L. 1988
X-ray emission from clusters of galaxies.
Cambridge University Press.

[29] Sommer-Larsen, J. 2004
Simulating Galaxies and Galaxy Clusters.
astro-ph/0404023 v1

[30] Sommer-Larsen, J., Romeo, A. and Portinari, L. 2005
Simulating Galaxy Clusters -III: Properties of the intracluster stars.
MNRAS, 357, 478

[31] Sommer-Larsen, J., Gotz, M. and Portinari, L. 2003
Galaxy formation: Cold dark matter, feedback, and the hubble sequence.
ApJ, 596, 47

[32] Stiavelli, M. and Setti, G. 1993
Non-equilibrium motions in galaxies and gravitational redshift.
MNRAS, 262, L51.